AD NUMBER

AD805759

LIMITATION CHANGES

TO:

Approved for public release; distribution is unlimited.

FROM:

**Distribution authorized to U.S. Gov't. agencies and their contractors;
Administrative/Operational Use; 15 NOV 1966.
Other requests shall be referred to Air Force Technical Applications Center, Washington, DC.**

AUTHORITY

AFTAC ltr 25 Jan 1972

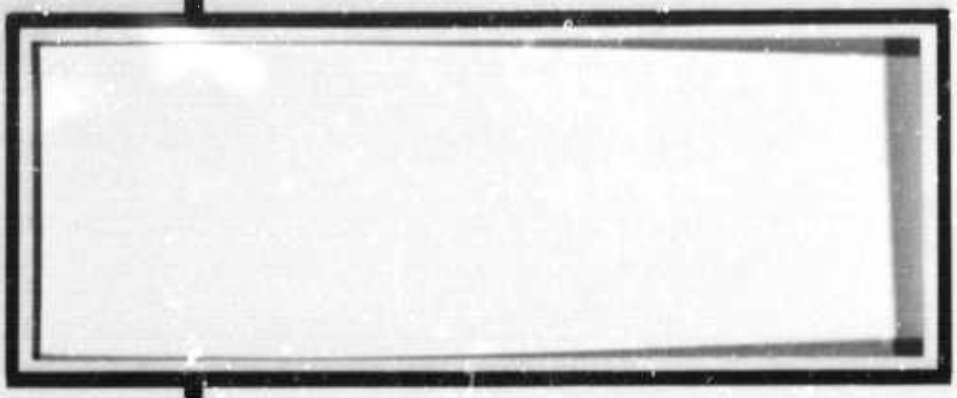

SCIENCE SERVICES DIVISION

TEXAS INSTRUMENTS
INCORPORATED

(9) Special rept.;

(6) ARRAY RESEARCH, SPECIAL REPORT NO. 18

AMBIENT NOISE ANALYSIS OF 3-COMPONENT SHORT-PERIOD DATA RECORDED AT TONTO FOREST SEISMOLOGICAL OBSERVATORY,

(14) TI-SR-18

Prepared by

(10) James A. Bonner
FL 7-5411, Ext. 221

TEXAS INSTRUMENTS INCORPORATED (347675)
Earth Science Programs
P. O. Box 5621
Dallas, Texas 75222

(15) Contract AF 33(657)-12747
Date: 13 November 1963
Expiration Date: 20 January 1967

Prepared for

AIR FORCE TECHNICAL APPLICATIONS CENTER
VELA SEISMOLOGICAL CENTER
Washington, D.C. 20333

ARPA Order-104-60
Project Code 8100

(11) 15 Nov[illegible] 66 (12) 64 p.

mt

mt

TABLE OF CONTENTS

LIST OF APPENDIXES

LIST OF ILLUSTRATIONS

LIST OF ILLUSTRATIONS (CONTD)

SECTION I

INTRODUCTION

This special report presents the results of a study of 3-component short-period ambient seismic noise recorded on the extended array at Tonto Forest Seismological Observatory (TFO) between 27 August 1965 and 1 September 1965. The object of the study is the evaluation of ambient noise characteristics to determine if substantial ambient noise variations (particularly in the trapped-mode components) exist across the extended array. The extent of such variations bears directly on the potential contribution of very-large-aperture short-period seismometer arrays to the nuclear blast detection and classification problem. The study was intended to provide:

- Evaluation of the data's validity to determine the feasibility of further analysis
- Determination of ambient seismic noise to system noise ratios
- Ambient seismic noise absolute spectral characteristics (at 20 station locations)
- Identification of obvious major noise types and/or sources

However, due to the inherent limitations of the data, absolute values can not be obtained for the spectra, and the determination of seismic noise to system noise ratios is not possible.

Of fundamental importance to multichannel filter system design and application at TFO are the ambient seismic noise field statistics as measured on a 3-component basis in the short-period frequency range. Accordingly, this study includes the determination of spectral shapes, inferences of time and space stationarity, and identification of dominant propagation modes. Inherent in these statistical characterizations are requirements for the analysis of recording and instrumentation system noise leading to determination of the usable seismic noise bandwidth of the recorded data.

The following section of this report briefly summarizes the analysis procedures and findings. The next sections describe the TFO large-aperture crossarray and instrumentation and the data recording systems. A detailed study of the analysis procedure is followed by a presentation of analysis results and a description of recommendations for further analysis of ambient noise at TFO.

SECTION II

SUMMARY

This section, which summarizes the ambient noise study, is divided into two parts:

- A brief description of analysis procedures and objectives
- Resulting conclusions

A. ANALYSIS PROCEDURES AND OBJECTIVES

Two noise samples from the short-period 3-component TFO data library* were chosen, based on usable seismic data for the most channels operating for an 8-min period. One noise sample was recorded when abnormally high surface winds prevailed; the other was recorded during a particularly quiet interval. Each noise sample had been gain-corrected by the Seismic Data Laboratory (SDL).

Preliminary power density spectra were computed on one noise sample for the vertical output of a van and for the vertical, radial and transverse components at a TFO installation. Artialiasing filtering and 2-to-1 resampling were performed on both noise samples, based on evaluation of these preliminary noise spectra.

A spectral analysis was performed on the resampled noise data. These spectra were used to interpret time and space stationarity, to determine the usable seismic bandwidth and to display the ratio of ambient seismic noise to system noise.

A coherence analysis was performed on the quiet noise sample. Coherence functions were computed between selected vector pairs and between vertical and radial, vertical and transverse, and radial and transverse components at selected stations. The coherence functions were interpreted for noise isotropy and types.

Analog bandpass frequency filters were applied to the time traces of the noise samples in order to identify dominant propagation modes. Velocities, directions and periods were determined for observed wave types from the filtered data.

---

*Texas Instruments Incorporated, 1966: Array Research Semiannual Tech. Rpt. No. 5, Sec. VII, AF 33(657)-12747, 1 Jul.

Baker, G. T., J. Hoffmann and T. Scherbal, 1966: Array Research Spec. Rpt. No. 12, Data Collection, Texas Instruments Incorporated, AF 33(657)-12747, 8 Apr.

B. CONCLUSIONS

The validity of the 1965 TFO crossarray noise data has been verified by comparison with 1963 noise data. However, due to contamination by broadband instrumentation noise, the van data were found to be of little use in conjunction with TFO data.*

It has been determined that gain corrections of the noise samples are unreliable, making absolute spectral magnitudes unattainable.* Therefore, the seismic noise to system noise spectral ratios were not computed.

Over the usable seismic bandwidth from about 0.1 to 1.3 cps (10 to 0.77 sec), the TFO noise spectra show only minor variations in spectral shape for like components within a noise sample. All noise spectra peak within the 4-sec to 6-sec microseism range. This similarity in spectral shape at all points within the array suggests that the noise field may be space-stationary. However, the lack of absolute spectral magnitudes prevents definite conclusions. The similarity of the 1963 and 1965 noise spectra indicates a degree of time stationarity in the noise field--again, somewhat speculative due to the unreliable gain corrections.

Analog bandpass filtering of the quiet noise displayed Rayleigh and Love wave energy in the 4-sec to 6-sec microseism band traveling toward approximately N40°E with a velocity of 3.5 km/sec. Frequency filtering of the windy noise displayed little evidence of this trapped-mode energy. In a previous TFO noise analysis,** the presence of low-velocity Rayleigh and Love wave energy was shown to be traveling from N60°E.

The ambient noise, although displaying very similar spectra at the TFO stations, was found to possess no significant coherence for receiver separations of 10 and 66 km, except for some highly coherent lines in the 4-sec to 6-sec range of the spectra for the quiet noise. Over the frequency range of interest, receiver separations were such that coherences significantly greater than zero could be expected only in a highly directional noise field or on horizontal instruments oriented along their separation vector in an isotropic noise field.

---

*Texas Instruments Incorporated, 1966: Array Research Semiannual Tech. Rpt. No. 5, Sec. II, AF 33(657)-12747, 1 Jul.

**Texas Instruments Incorporated, 1965: Array Research Semiannual Tech. Rpt. No. 3, Sec. VI, AF 33(657)-12747, 3 Jun.

The horizontal seismometer in line with the 4-sec to 6-sec energy shows a high coherence with the vertical seismometer in that frequency range, but the transverse horizontal seismometer has very small coherence with either. This is additional evidence that the energy is Rayleigh motion. The presence of Love wave energy on the transverse seismometer can be inferred from its arrival pattern and lack of coherence with other seismometers. It was not possible to determine the power relationship between the Rayleigh and Love wave modes due to the absence of absolute spectral values.

Tropical storm Emily, which was positioned off the lower Pacific Coast of Baja California during the recording of the quiet noise sample, generated the Rayleigh and Love wave energy. The remaining energy in the usable seismic band of both noise samples is nonisotropic bodywave noise coming from a predominantly southwest direction. The bodywave noise is observed to be traveling at velocities of 8 km/sec or greater in the frequency band of 0.25 to 1.2 cps.

SECTION III

TFO LARGE-APERTURE ARRAY

The twelve 3-component short-period installations at TFO were augmented by eight standard Geotechnical Corporation LRSM mobile vans to form an extended large-aperture array. Four of the vans were located on an approximate N53°W line and four on an approximate N37°E line, as shown in Figure 1. A standard Geotechnical Corporation 3-component short-period system consisting of vertical, radial and transverse components was installed at each van. The instruments were 1.0-sec Benioff seismometers connected to a phototube amplifier (PTA) operated with a 0.2-sec galvanometer and a 0.01- to 10.0-cps bandpass filter. A 3-component system consisting of vertical, radial and transverse components (Figure 2) was installed at selected locations of the TFO crossarray. The instruments were 1.25-sec Johnson-Matheson seismometers connected to a PTA operated with a 0.33-sec galvanometer and a 0.01- to 10.0-cps bandpass filter. All seismometers were oriented with respect to the Nevada Test Site (NTS). The van instruments were oriented such that a compressional wave arriving from the north would produce a positive voltage output on each instrument of the system (Figure 1). The TFO instruments produced a positive voltage output for a compressional wave arriving from the west (Figure 2).

Each leg of the extended array is approximately 200 km in length and thus spans a large geological area. In Figure 3, there is some indication of the wide variations in geology over the extended array.

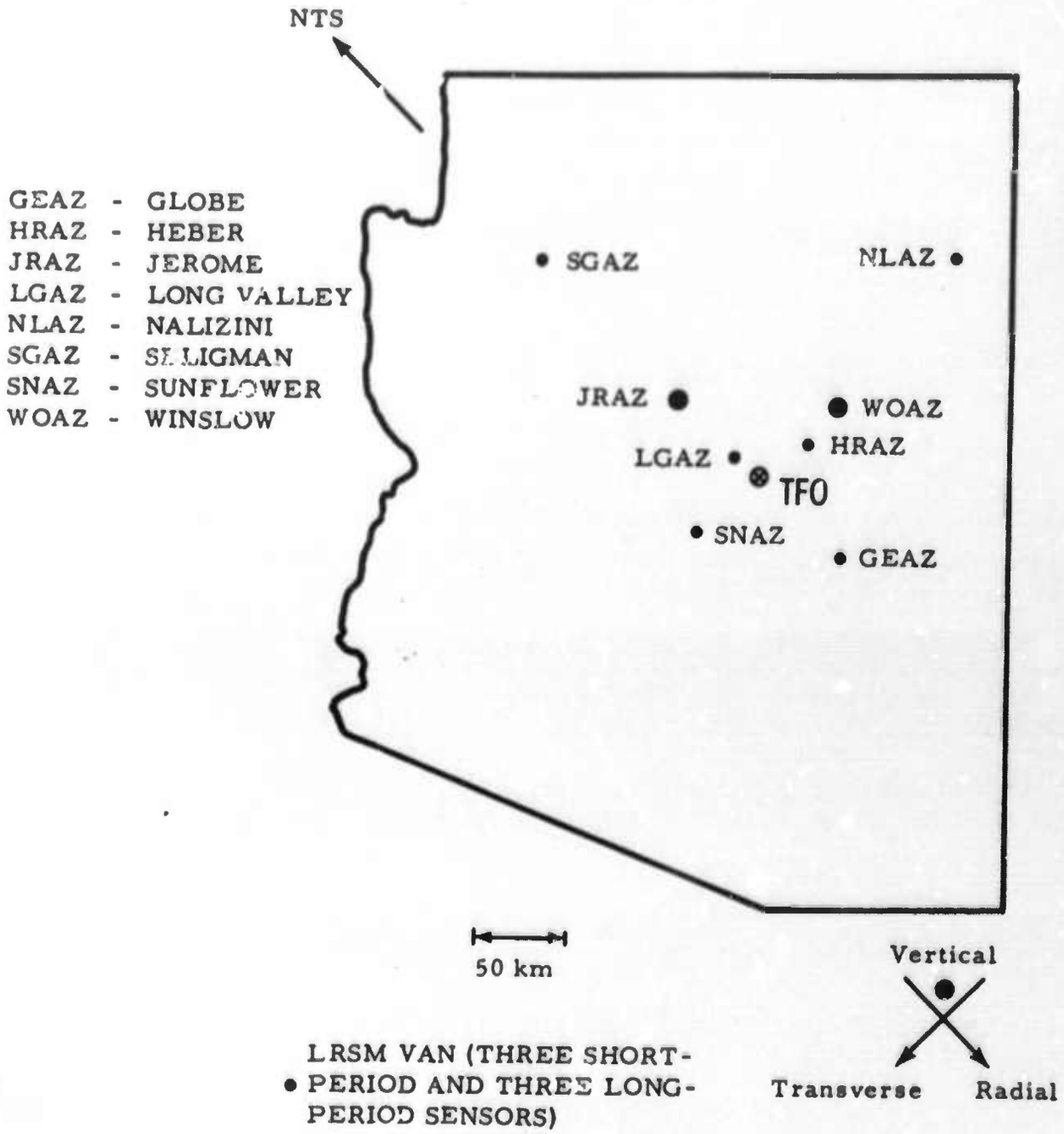

Figure 1. Configuration of Extended TFO Sensors

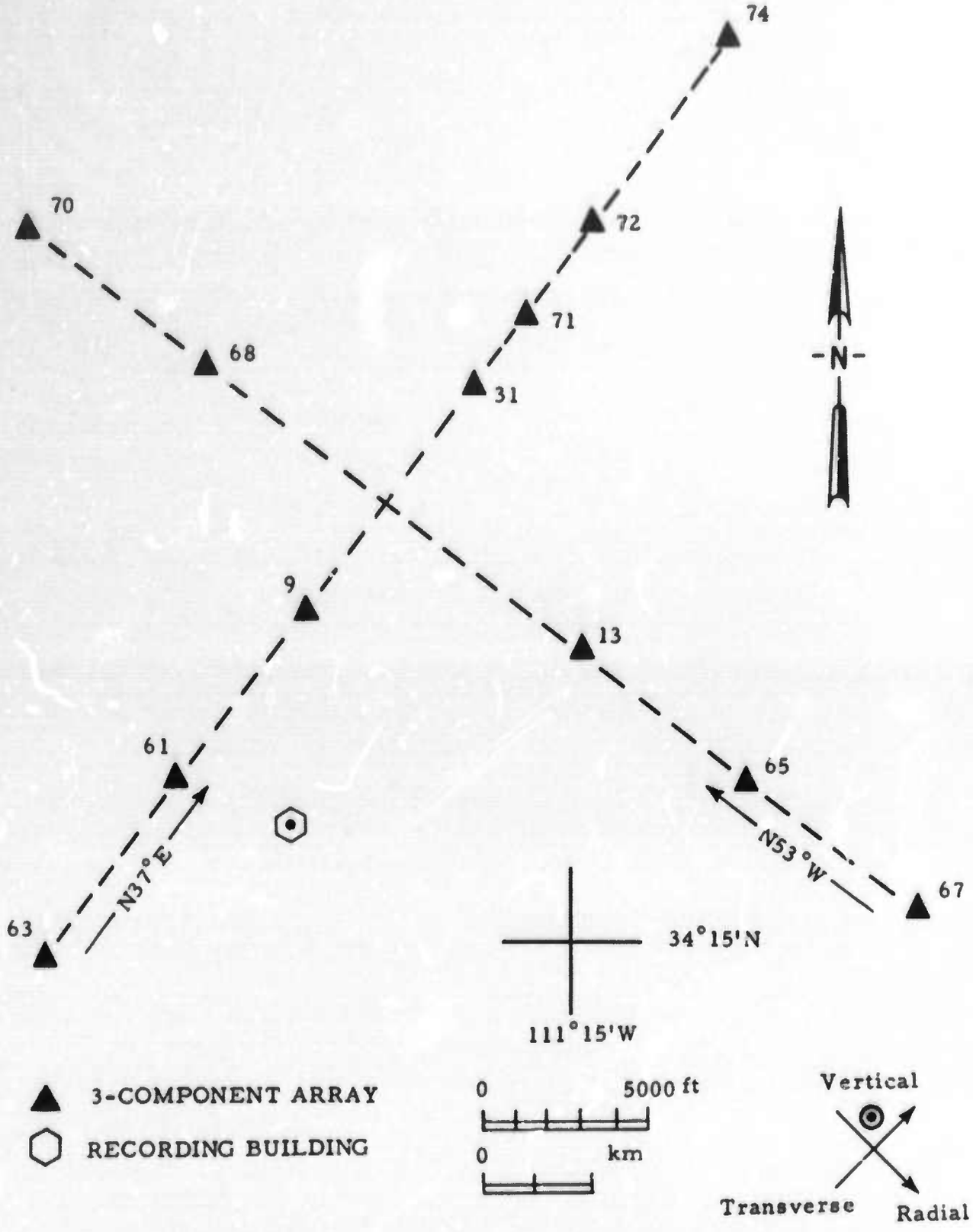

Figure 2. TFO 3-Component Seismometer Locations

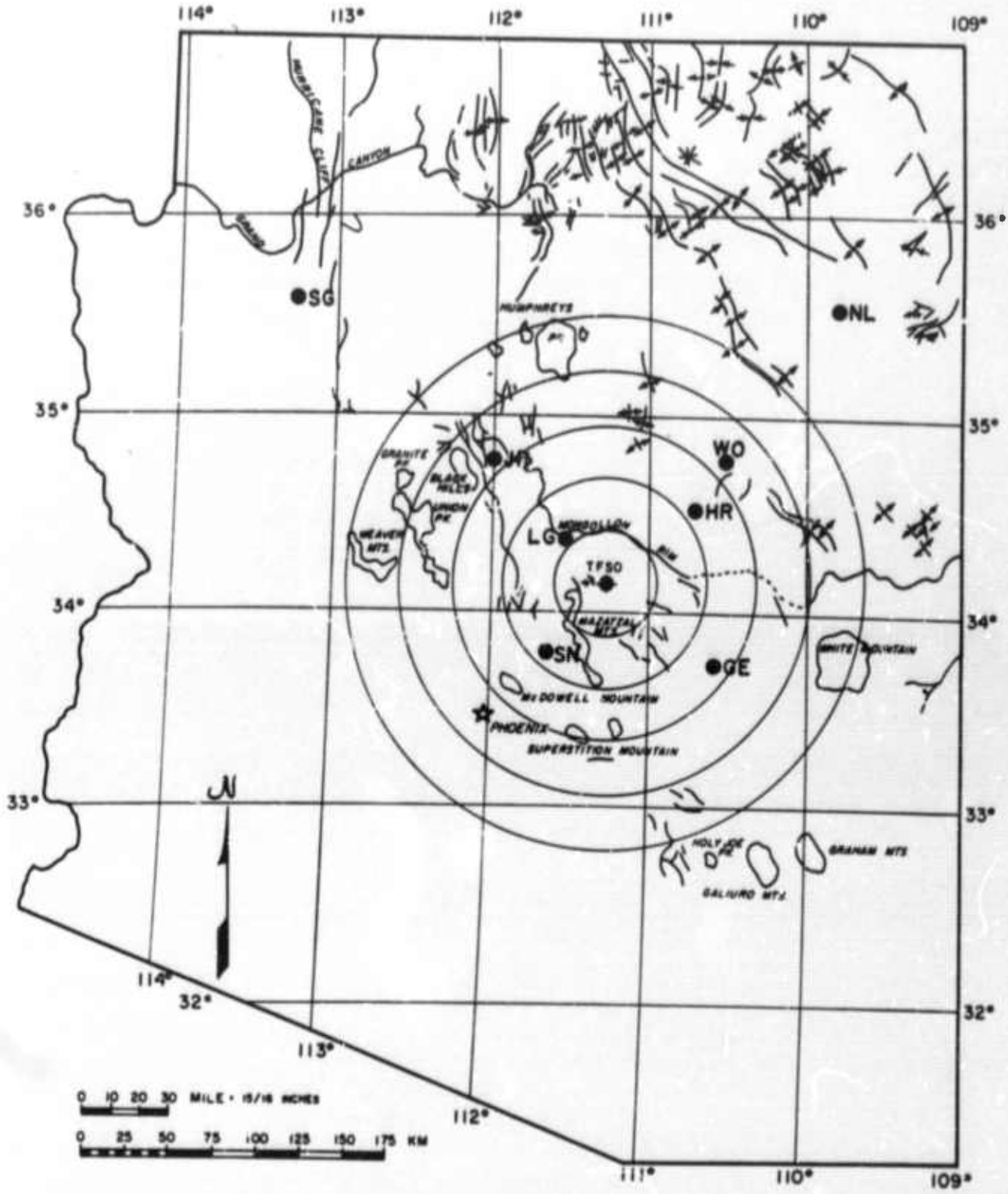

Figure 3. Geological Summary of Extended TFO Array Locale

SECTION IV

TFO DATA RECORDING SYSTEM

Figure 4 is a block diagram of the data and recording systems for the 3-component short-period array at TFO. Outputs from the Benioff seismometers and associated short-period phototube amplifiers (PTA) at the vans were directed to Astrodata telemetry voltage-controlled oscillators (VCO) for input to the Bell System and transmission to TFO. Four channels of data were transmitted from each of the eight vans (one channel for each instrument and one test channel). Data recovered from Astrodata telemetry demodulators at TFO were sent to the station Develocorders and through variable-gain operational amplifiers to the Astrodata Data Acquisition System.

Outputs from the TFO Johnson-Matheson seismometers and associated phototube amplifiers were passed through operational amplifiers to the station distribution system and through isolation amplifiers and variable-gain operational amplifiers to the Astrodata Data Acquisition System.

The variable-gain amplifiers used on the input of the Astrodata Data Acquisition System were installed especially for the Texas Instruments data recording so that ambient seismic noise could be recorded at a sufficiently high level to make best use of the available dynamic range of the digital system. As indicated by the capacitors shown in Figure 4, a-c coupling also was especially installed to prevent restriction of the digital system's available dynamic range by d-c offsets (developed at the PTA and telementry demodulator outputs). The restricted low-frequency response provided by the a-c coupling also served to diminish the effects of very low-frequency drifts in the PTA and telemetry outputs.

Due to the inherent limitations of the recording system, two types of system noise, in addition to the desired data, were recorded on the Astrodata Data Acquisition System tapes. The noise types are telemetry and Astrodata system noise, the latter including Astrodata quantization noise. Figure 4 shows equivalent input points for these noise types, and Figure 5 shows their level at the input points.

The theoretical Astrodata quantization noise level is assumed to be 66 db below clipping level; i.e., the least significant bit level is assumed to represent the quantization noise level. The Astrodata system noise level is estimated to be no lower than -60 db and is assumed to be white although it has not been measured.

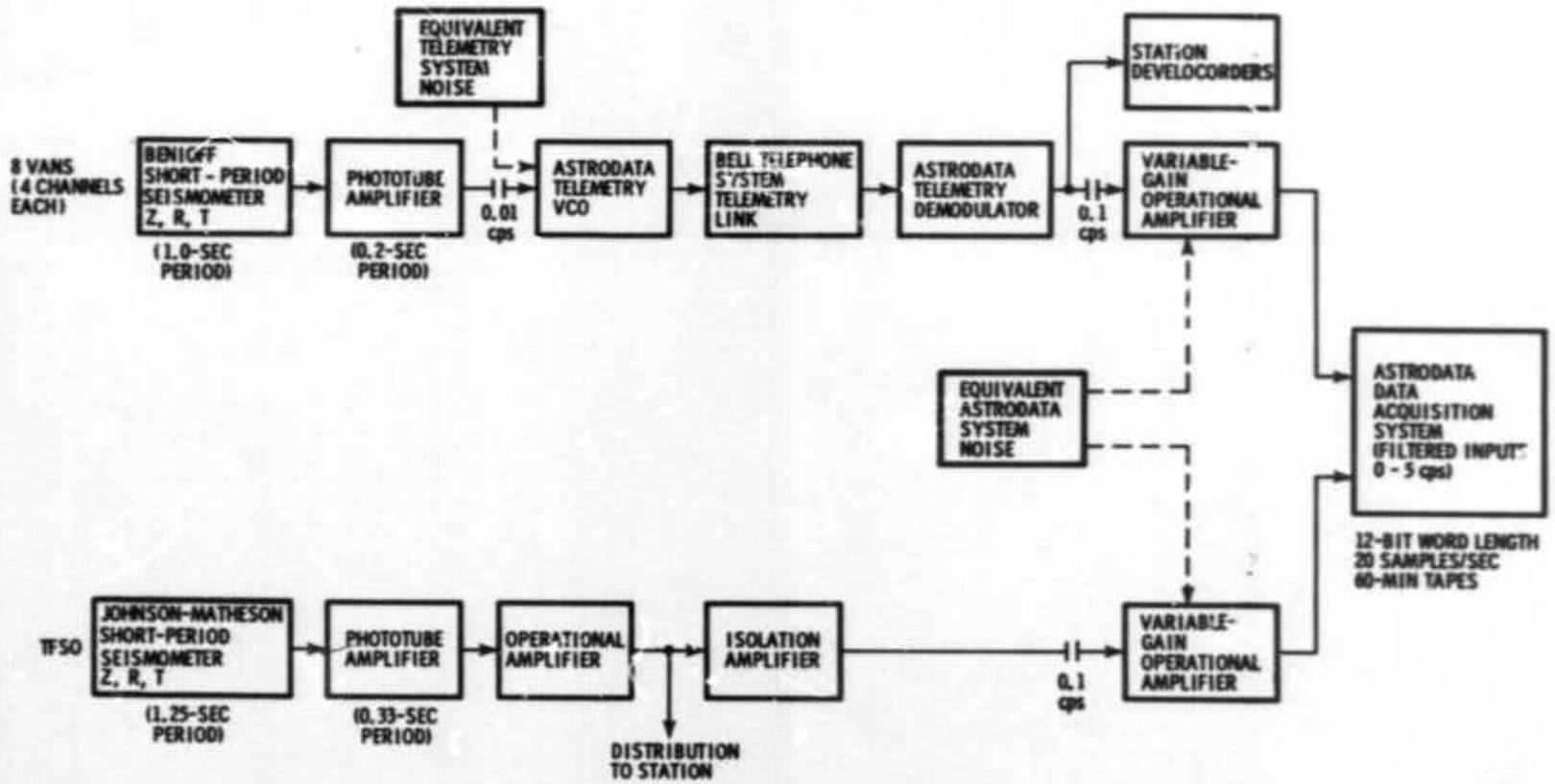

Figure 4. Block Diagram of Data and Recording Systems for Short-Period Large-Aperture Array at TFO

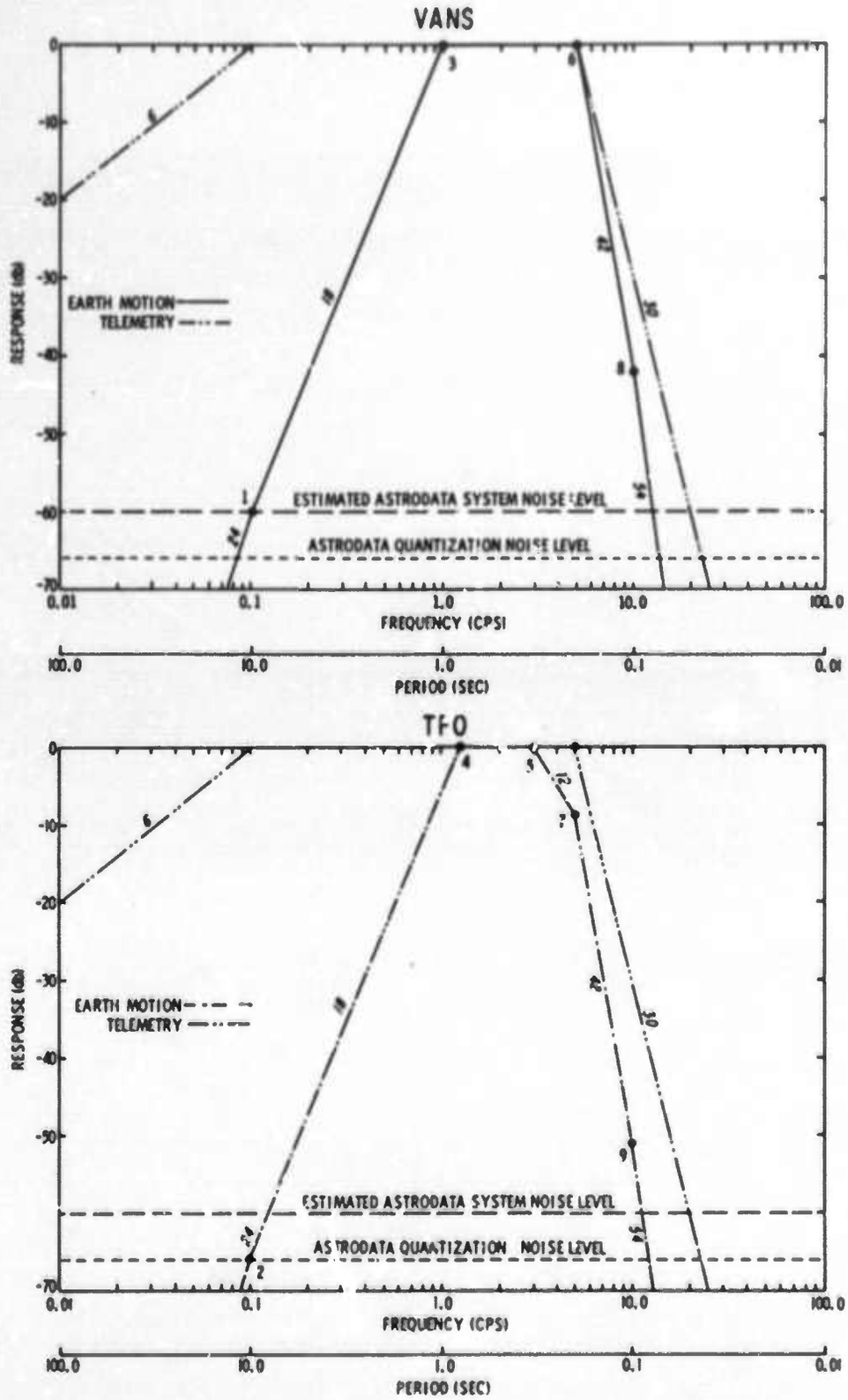

Figure 5. Recording System Composite Response to Earth-Motion (Seismic) and Telemetry Noise Inputs

The Astrodata quantization noise level is inherent in the Astrodata system and is presumed to be recorded as a white noise component having no frequency filtering. The Astrodata system noise, which is developed within the input circuitry to the Astrodata system, is presumed to be filtered before recording by the system antialias filters, which have zero attenuation from 0 to 5 cps and 30 db/octave rejection above 5 cps. Hence, Astrodata system noise is recorded as a white component from 0 to 5 cps.

Figure 5 shows the theoretical asymptotic responses of the recording system to telemetry noise and to earth-motion input at the seismometers. The number located by each branch of the responses gives the rate of change of response in db/octave. Also, the Astrodata noise level and the Astrodata quantization noise level are indicated.

The telemetry noise response has breakpoints at 0.1 and 5 cps (10 and 0.2 sec) due to a-c coupling and the input filters to the Astrodata system, respectively. Thus, the telemetry noise is passed with zero attenuation from 0.1 to 5 cps (10 to 0.2 sec).

The recording system's response to an earth-motion input to the seismometer displays a 60-db dynamic range over a bandwidth of approximately 0.1 to 12 cps (10 to 0.08 sec) for the assumed Astrodata system noise level. Figure 5 shows the breakpoints of the seismometer responses for the vans and TFO. Breakpoints 1 and 2 are due to the a-c coupling networks. The 1.0-sec and 1.25-sec seismometers are associated with breakpoints 3 and 4, respectively, at 0 db. The TFO 0.33-sec PTA galvanometers cause breakpoint 5. Breakpoint 6 results from both the Astrodata filters and the van 0.2-sec PTA galvanometers, and breakpoint 7 is due to the Astrodata filters. The PTA bandpass filters cause breakpoints 8 and 9.

SECTION V

PREPROCESSING SHORT-PERIOD DATA

Data from the TFO short-period extended array were recorded by the Astrodata system on IBM-format tapes which were reformatted by the Seismic Data Laboratory (SDL) computers. Figure 6 is a block diagram of the processes performed by SDL.

The TFO Astrodata tapes, digitized at 20 samples/sec, underwent an editing process in which specified events were physically located on the tapes. An autocorrelation calibration analysis was performed on calibration tapes from TFO to determine the counts that the Astrodata system generated per millimicron of earth motion (c/mμ) at 1.0 cps for each seismometer. Then, multipliers were computed and applied to gain-correct all seismometers at 1.0 cps to 90 c/mμ for low-gain data and 180 c/mμ for high-gain data.

Gain-corrected events then were reformatted into TIAC* (Texas Instruments Automatic Computer) compatible IBM tapes which were subsequently translated into TIAC-format tapes for further processing.

Paper playbacks for each event, together with all pertinent information, were placed in the TFO short-period data library.** The reformatting process proved to be satisfactory for converting data from TFO Astrodata-format tapes to TIAC-format tapes; however, the calibration analysis process did not result in properly gain-corrected data.**

---

* Trademark of Texas Instruments Incorporated

** Texas Instruments Incorporated, 1966: Array Research Semiannual Tech. Rpt. No. 5, Sec. VII, AF 33(657)-12747, 1 Jul.

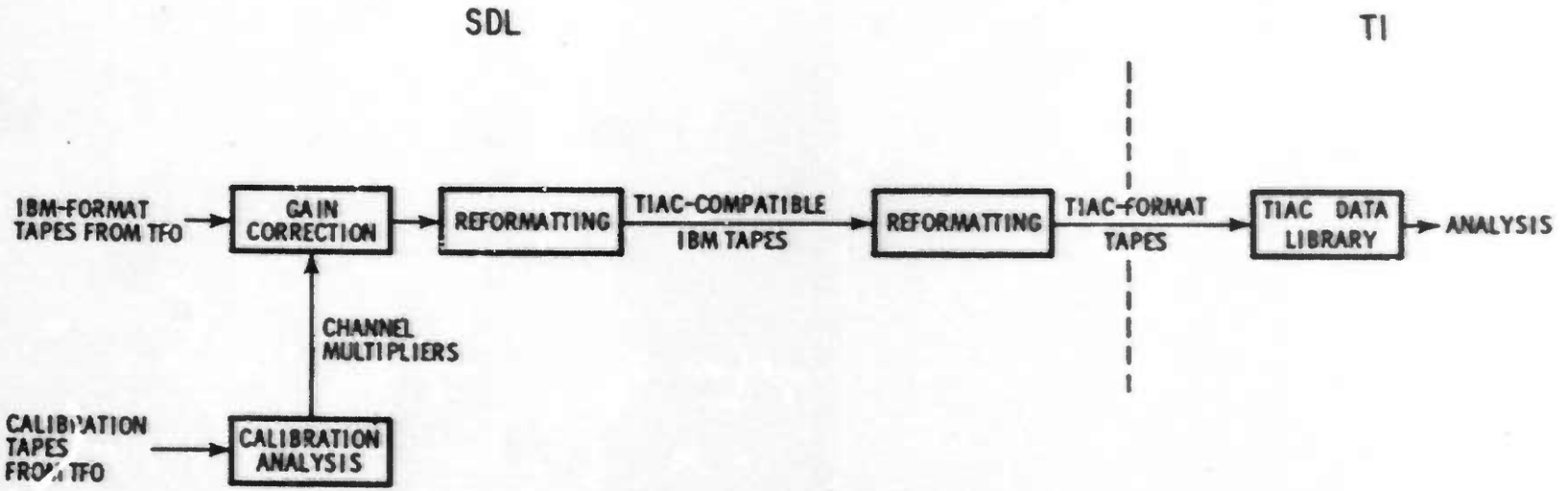

Figure 6. Block Diagram of Data Processing Operations Preceding Texas Instruments Analysis

SECTION VI

TIAC DATA ANALYSIS

This section details the data processing involved in the TFO short-period ambient noise study. Figure 7 is a summary flow chart of the analysis.

A. DESCRIPTION OF NOISE SAMPLES

Two 8-min noise samples (NSH-1F and NSH-36)* were chosen from the TFO data library. The data were sampled at 50-msec intervals, for a total record length of 9600 points. Noise sample NSH-1F was recorded on 27 August 1965 at 05:15:30 GMT when abnormally high surface winds prevailed; noise sample NSH-36 was recorded on 1 September 1965 at 06:15:00 GMT during a particularly quiet period. The latter is probably more typical of average TFO noise.

Noise samples were chosen on the basis of usable seismic data for the most channels operating for an 8-min period. Omitted from the analysis were channels with nonseismic noise, clipping and numerous spikes. Noise sample NSH-1F has 55 usable channels out of 60, and noise sample NSH-36 has 52 usable channels.

B. ANALYSIS

A preliminary high-resolution power density spectral estimate was computed over the full Nyquist band (0 to 10 cps) for the output of a vertical component of a van and for vertical, radial and transverse components at a TFO installation. It was determined that antialiasing filtering above 5 cps and 2-to-1 resampling would be acceptable.

A 50-point, digital, minimum-phase, antialiasing filter was designed to provide a gain of unity in the passband from 0 to 4 cps, to follow a cosine function from 4 to 5 cps, and to maintain a constant gain of 0.001 from 5 to 10 cps. Figure 8 shows amplitude and phase responses. The two noise samples were filtered and 2-to-1 resampled, yielding data sampled at 100-msec intervals, for a total record length of 4800 points. Power density spectra were calculated for all available channels of each noise sample. Appendix A contains the power density spectra of the resampled data.

Interpretation of the spectra was made for time stationarity; space stationarity; and spectral shape and magnitude.

---

*Ibid (pertaining to the classification system used for events in the TFO short-period data library).

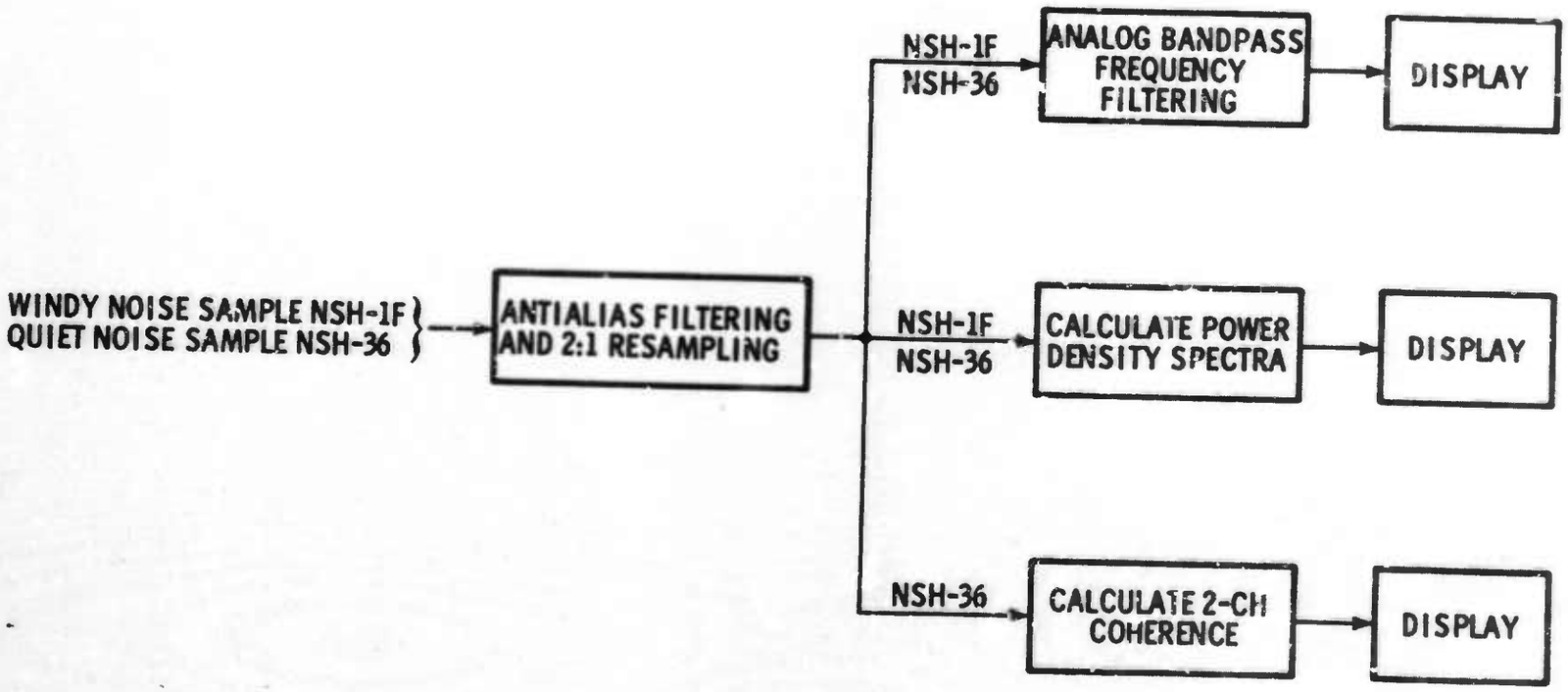

Figure 7. Flow Chart of TIAC Data Analysis

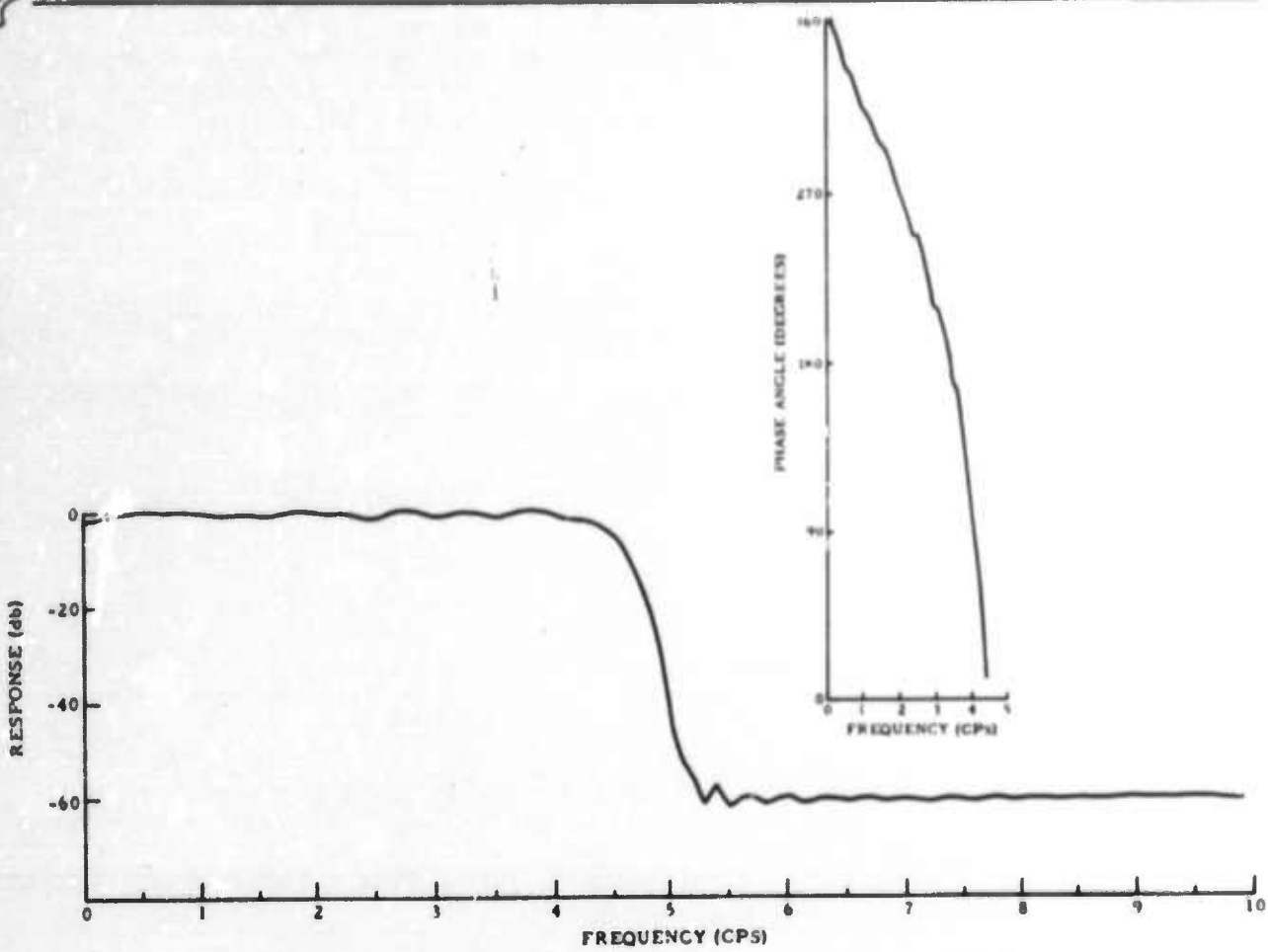

Figure 8. Amplitude and Phase Responses of the 5-cps Antialias Filter

To evaluate the structure of the ambient noise, analog bandpass filters were applied to both noise samples to isolate the contents of several frequency bands. The analog bandpass filters have an attenuation of 18 db/octave outside the passband and a constant gain in the passband. Filters with the following passbands were applied and interpreted: 0-0.2 cps, 0.21-0.57 cps, 0.48-0.92 cps and 0.90-1.20 cps. Appendix B displays the results of the filtering.

High-resolution (12.4-sec correlations) coherence functions were computed at three locations, using the resampled quiet noise (NSH-36). The selected locations were the Heber van (nearest to the TFO crossarray on the N37°E arm) and Z74 and Z63 at opposite ends of the N37°E arm of the TFO crossarray. At Heber and Z74, coherences were computed between the vertical and radial, the vertical and transverse, and the radial and transverse components. Coherences also were computed between Heber and Z74 and between Z74 and Z63 for the respective vertical, radial and transverse components. Coherence functions were interpreted for directional wave types.

SECTION VII

ANALYSIS RESULTS

Analysis of the ambient noise field at TFO as recorded by the short-period extended array was performed by computation of power density spectral estimates and coherence functions and application of analog bandpass filters to the noise time traces. Results of the analysis are described in ~~the following paragraphs~~ this report.

Figures 9 through 14 display short portions of 3-component data from each noise sample recorded at a sample rate of 50 msec. A distinct difference between the quality of the van data and that of TFO is observed. The van data, telemetered to TFO over telephone lines, evidently contain broadband transmission or other system noise which distorts or obscures the seismic data. TFO data appear to be of good seismic quality but are not properly gain-corrected.

A preliminary high-resolution power density spectral estimate was computed from the quiet noise sample (NSH-36) over the full Nyquist band (0 to 10 cps) for the vertical component output of a van (GE Z) and the vertical, radial and transverse components at TFO installation Z61. These spectra, displayed in Figure 15, indicate the presence of very little energy above 5 cps in the recorded data because of the input filters to the Astrodata Data Recording System (Section IV). The noise samples were resampled 2 to 1 to provide records 4800 points in length with a 100-msec sample rate.

After the resampling, power density spectral estimates were computed for all usable channels of each noise sample (displayed in Appendix A).

As a demonstration of the validity of the present data, Figure 16 presents spectra of noise samples recorded from TFO instruments Z61 and Z72. These were first recorded on 20 December 1963 and again on 27 August 1965 and 1 September 1965. Although the 1963 data were prewhitened before spectral computation* and the 1965 data were not, the similarity between the spectra is apparent. Note particularly the correspondence of respective peaks at approximately 0.2, 0.6, 2.1, and 3.6 cps. The uncertainty of the gain correction of the 1965 data precludes comparisons of absolute spectral levels.

Figure 17 shows examples of two typical van spectra and two TFO spectra for the three components. The van spectra are generally whiter than are the TFO spectra and frequently contain extraneous peaks and other features that identify them as representing energy that is partly nonseismic. These van spectra indicate that either the data received by telemetry and recorded at TFO are contaminated with telemetry or other system noise or strong noise sources exist near all of the eight van installations.

* Texas Instruments Incorporated, 1965: Array Research Semiannual Tech. Rpt. No. 3, Sec. V, AF 33(657) - 12747, 3 Jun.

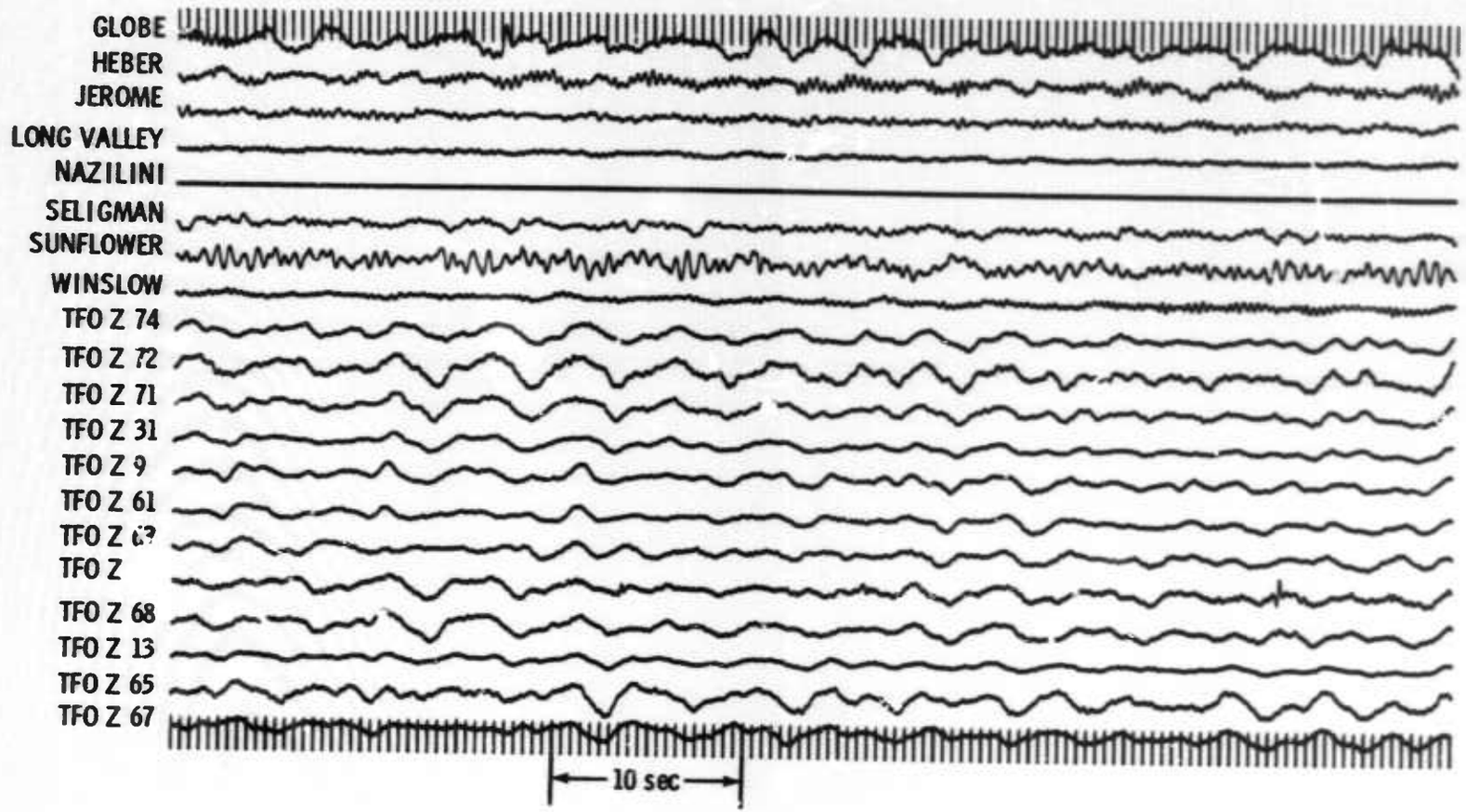

Figure 9. Quiet Noise Sample (NSH-36) Vertical Record

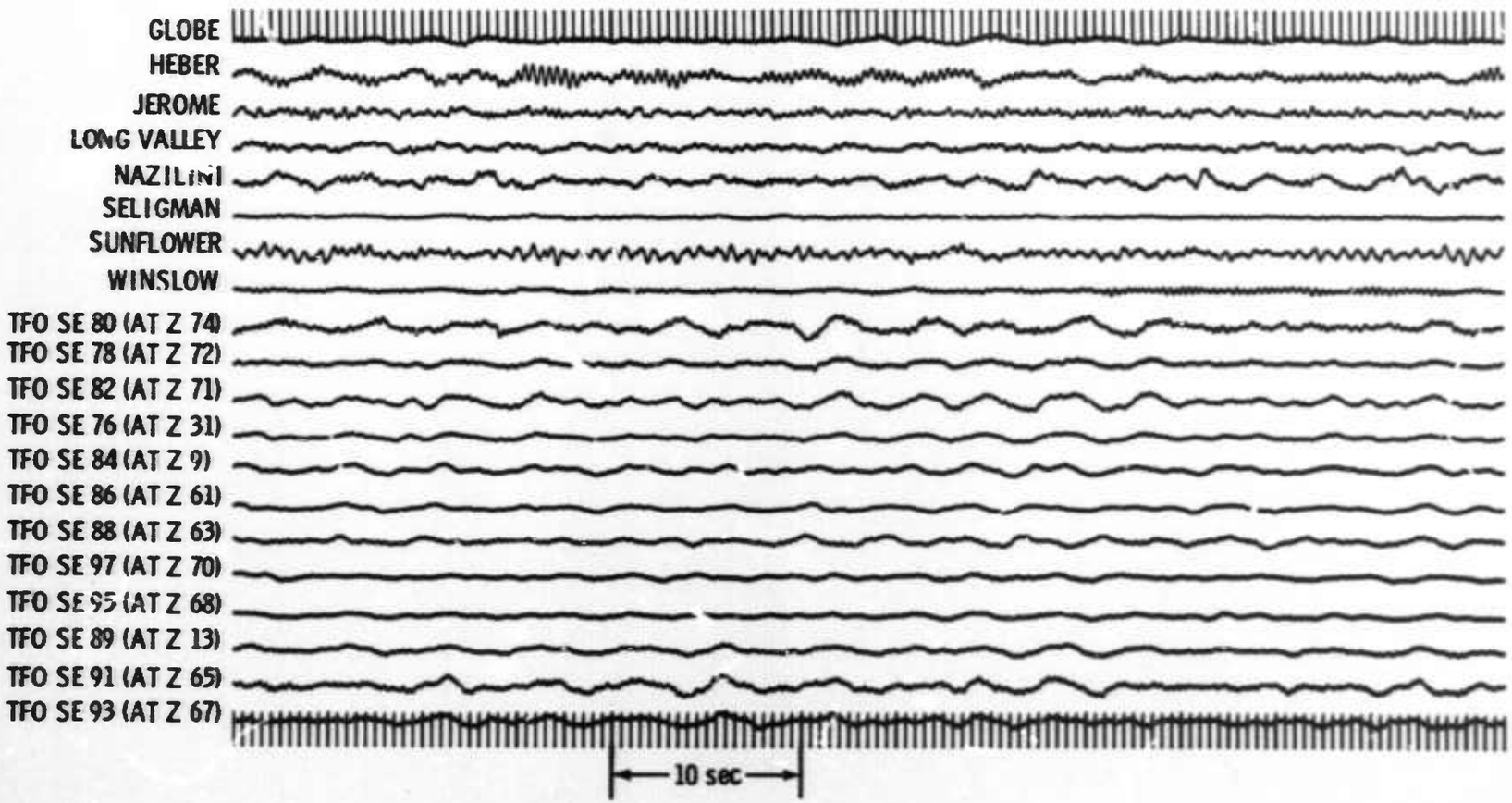

Figure 10. Quiet Noise Sample (NSH-36) Radial Record

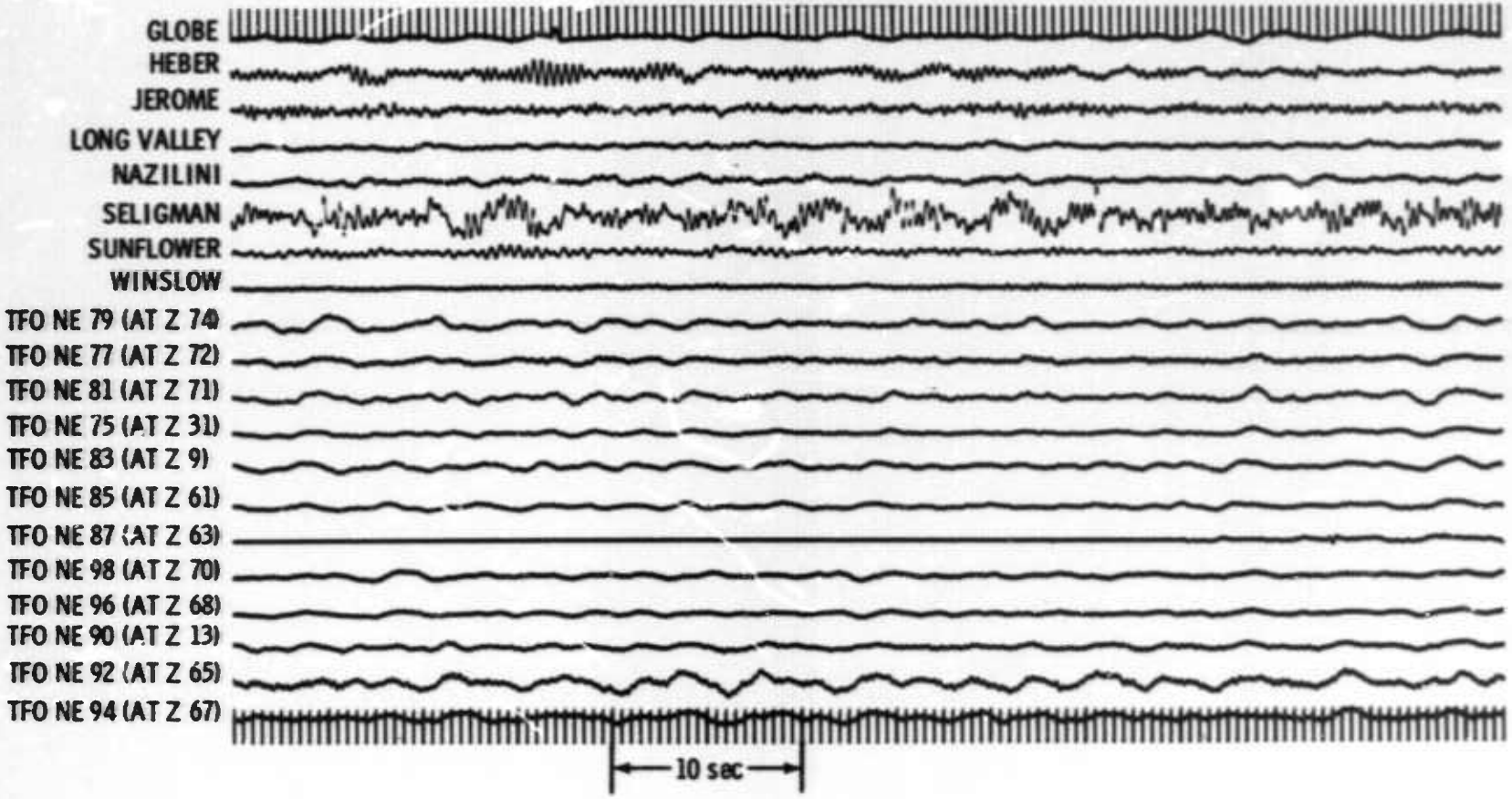

Figure 11. Quiet Noise Sample (NSH-36) Transverse Record

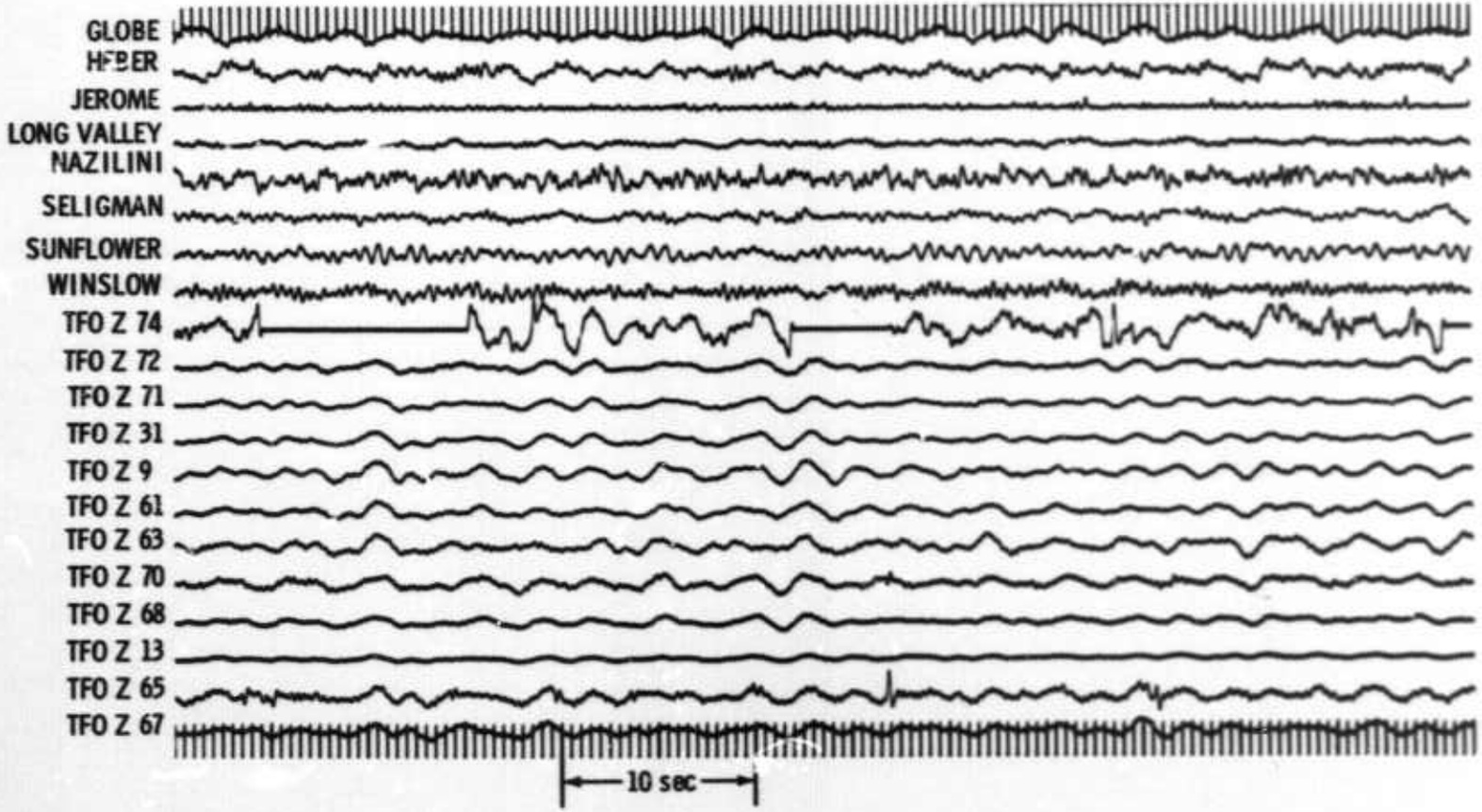

Figure 12. Windy Noise Sample (NSH-1F) Vertical Record

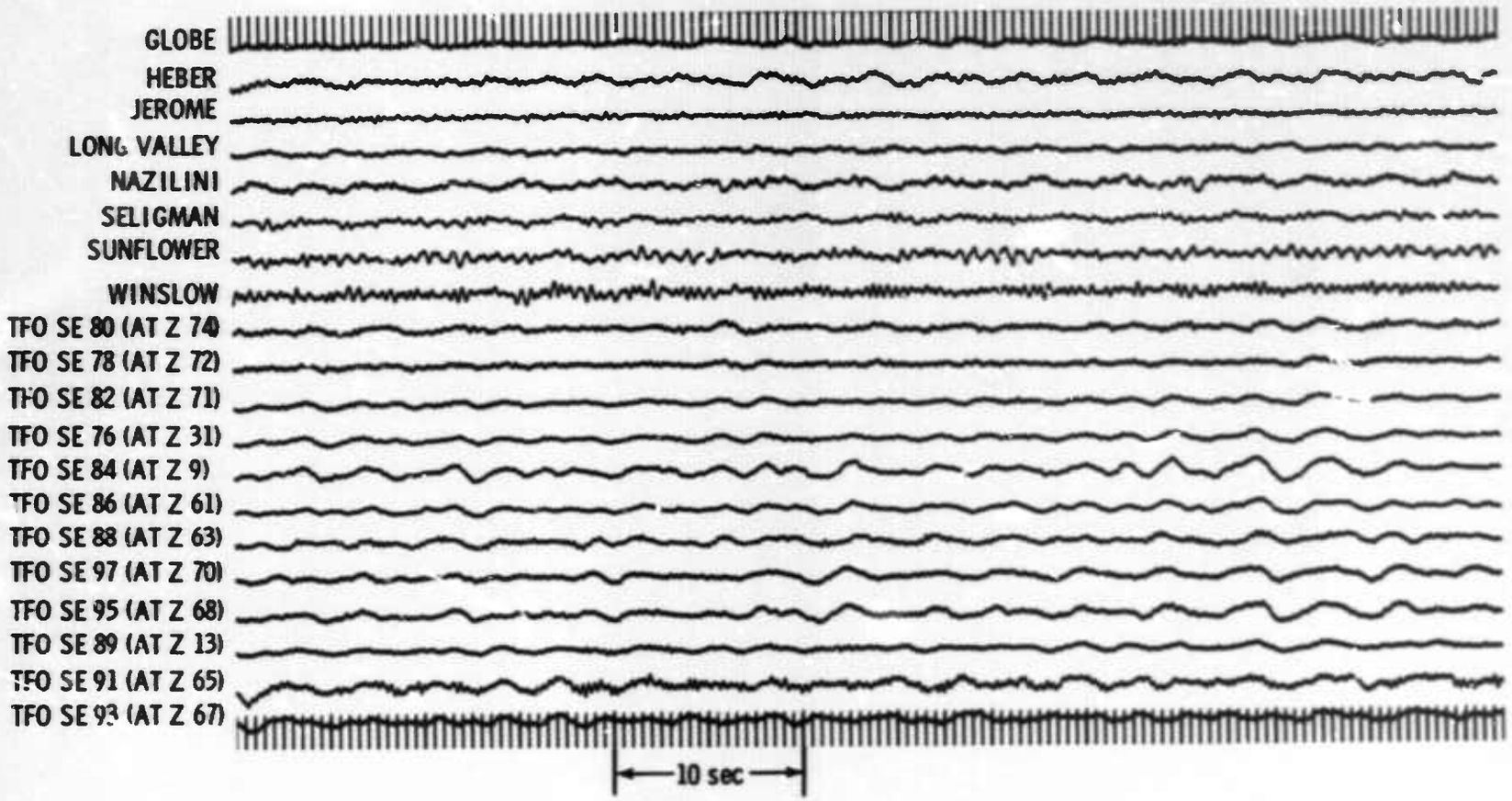

Figure 13. Windy Noise Sample (NSH-1F) Radial Record

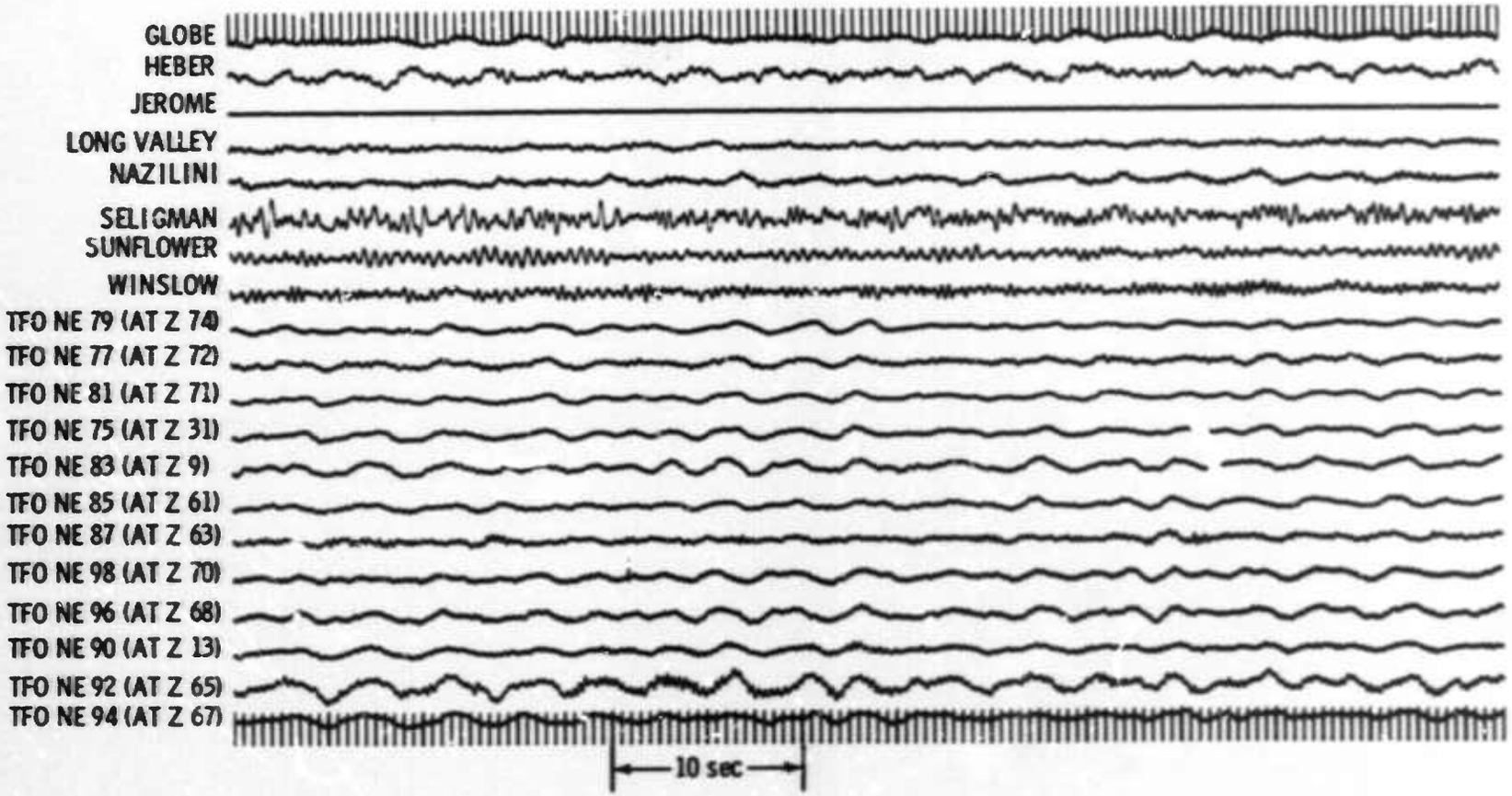

Figure 14. Windy Noise Sample (NSH-1F) Transverse Record

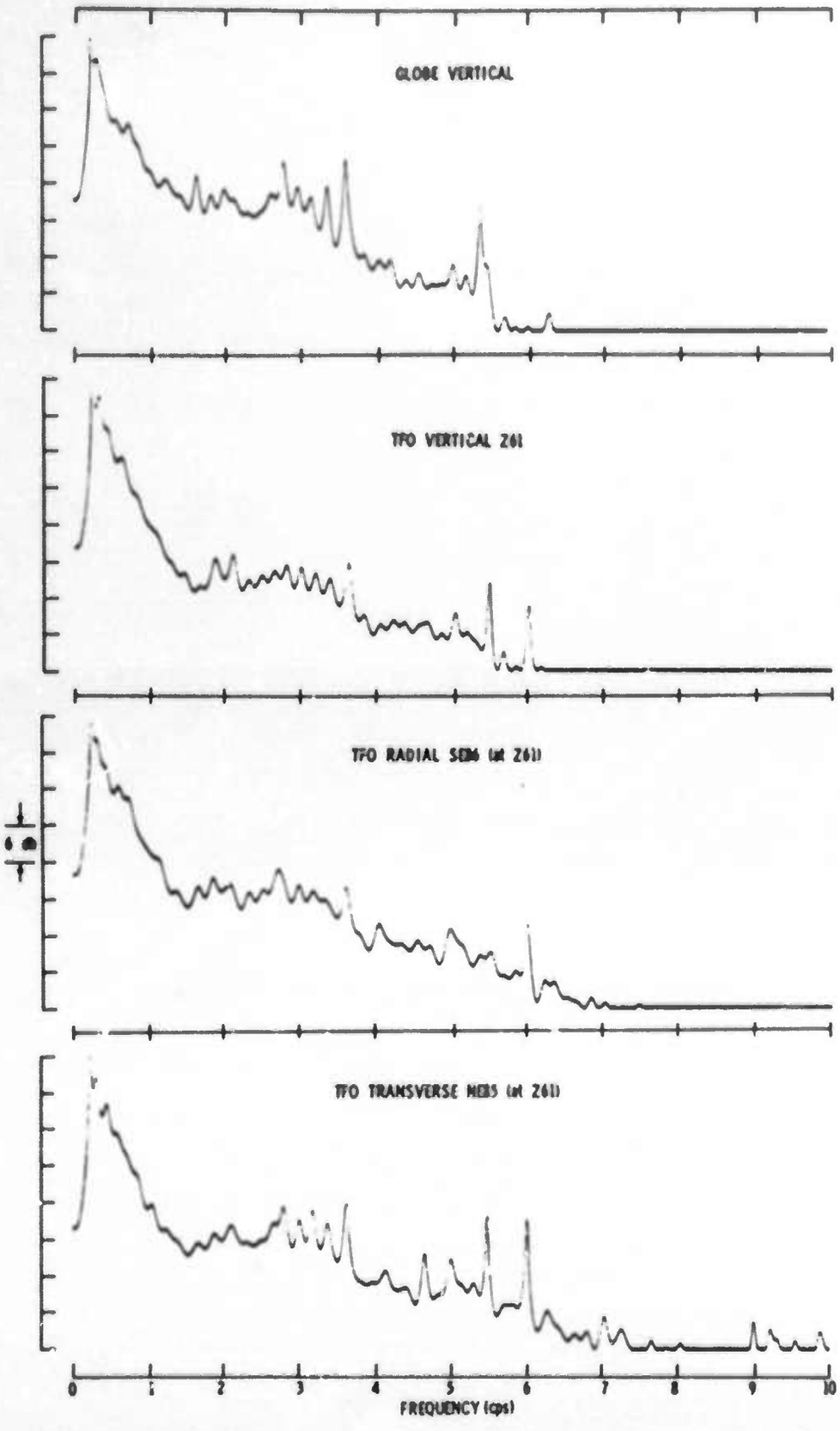

Figure 15. Power Density Spectra of Quiet Noise Sample (NSH-36) over Full Nyquist Band (0 to 10 cps)

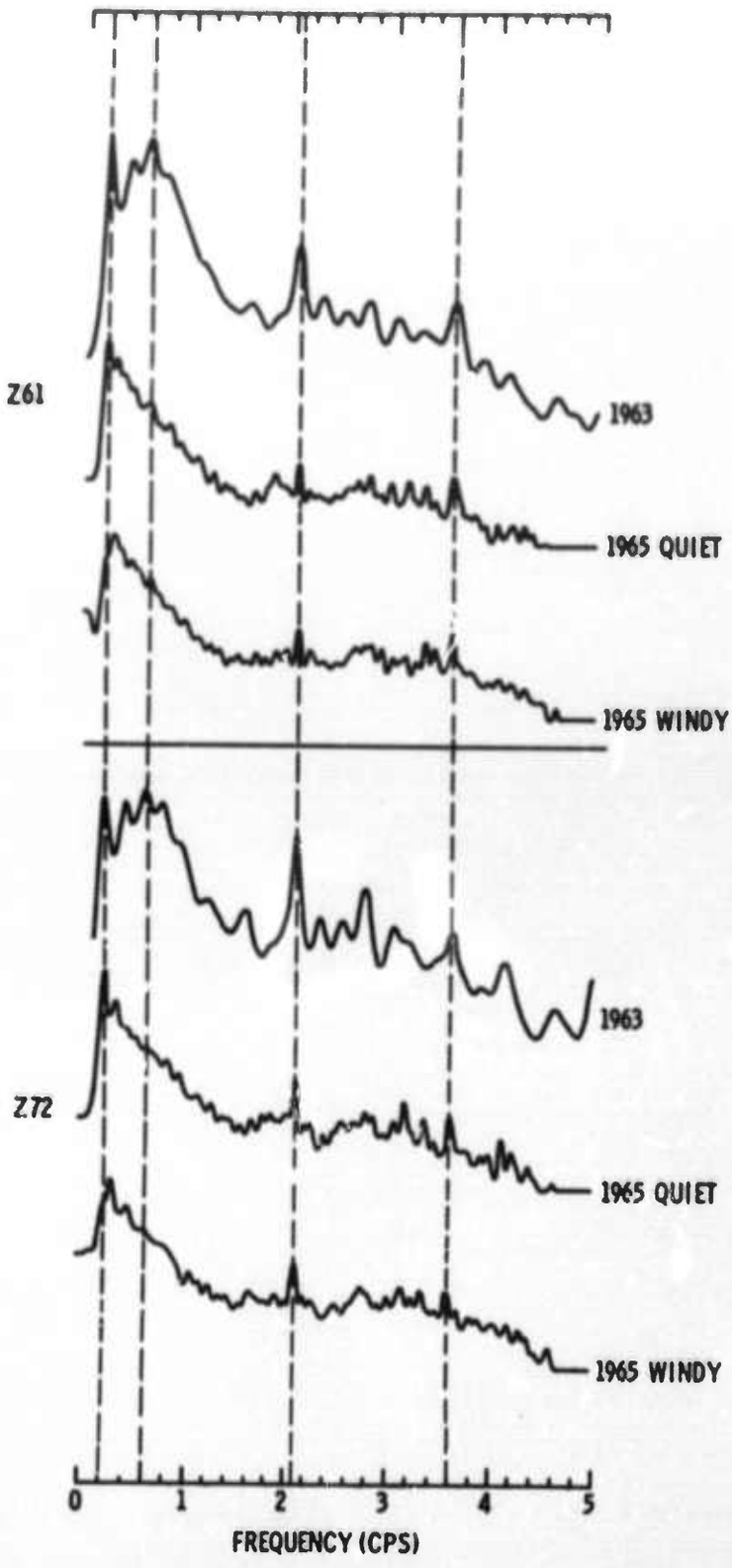

Figure 16. Comparison of TFO Spectra

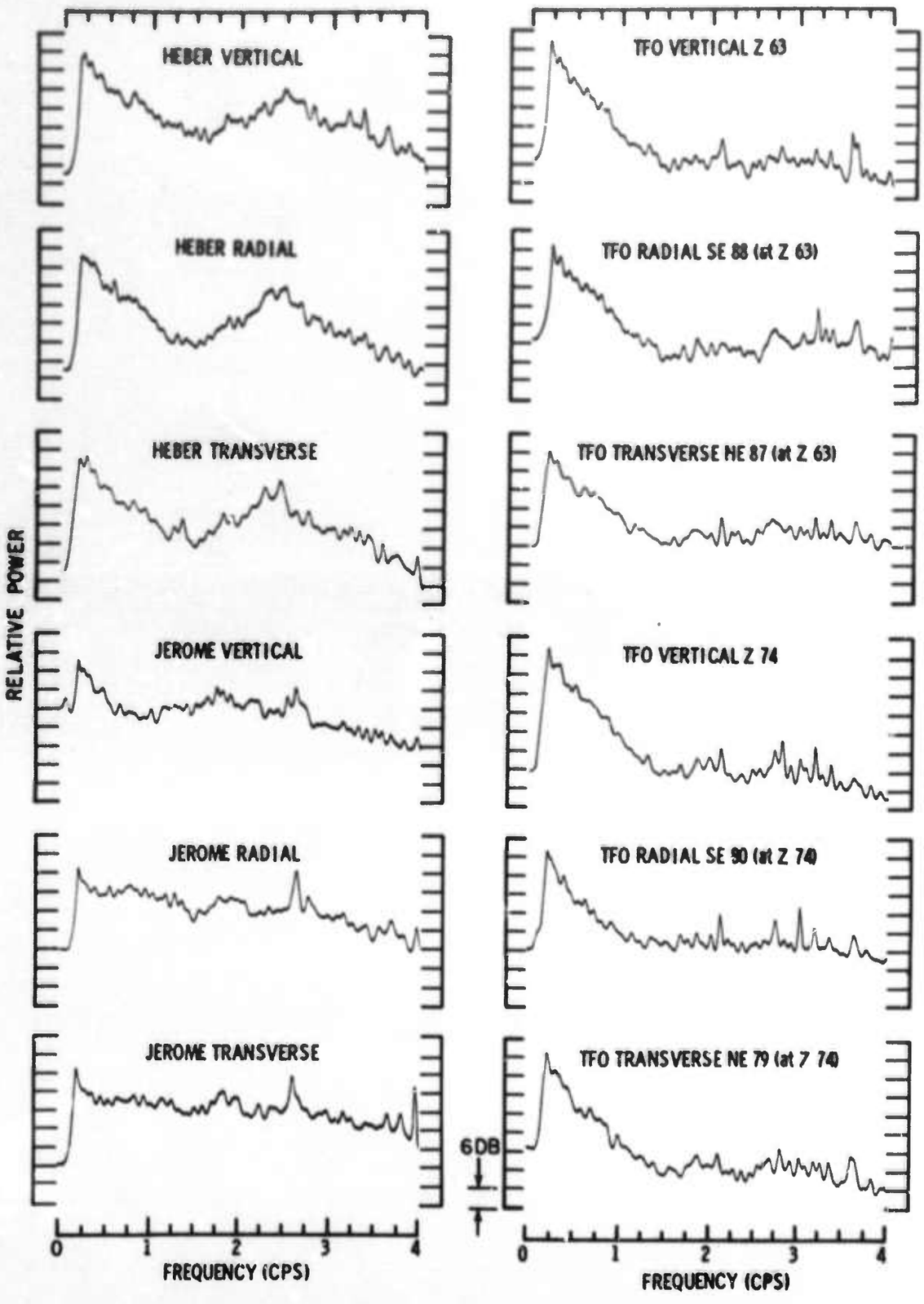

Figure 17. Examples of Typical Van and TFO Noise Spectra

In view of the low probability of the latter and the generally nonseismic appearance of the van data, use of the van data in conjunction with TFO data is not likely to produce valid results, and interpretation must be done with great care.

As discussed in Section II, gain correction of the short-period data is not believed to be reliable for all records,* making absolute spectral magnitudes unusable. Without absolute references for the spectra, the seismic noise to system noise spectral ratios for which this task provides would be meaningless. Consequently, such ratios were not formed. Spectra of system noise tests have not been computed because a comparison of van and TFO spectra (Figure 17) shows that, with most vans, system noise is obviously large enough to compromise the use of the van data. Comparison of the 1963 and 1965 TFO data (Figure 16) shows that the TFO system noise is low enough so that it does not hamper analysis.

The TFO array combined with the eight additional vans provided an array of approximately 200-km aperture. With such a large array, large variations in the ambient noise field are possible over the array, making it pertinent to attempt determination of major noise types, sources and locations. In view of the discovery that the van data are of limited or no use, the array is reduced effectively to a 10-km aperture centered at TFO; thus, the probability of significant variations in the noise field is considerably reduced, making the examination of specific noise sources more difficult.

Over the usable seismic bandwidth from approximately 0.1 to 1.3 cps (10.0 to 0.77 sec), comparison of spectra for all three components shows only minor variations in spectral shape from one location to another within the TFO crossarray, suggesting that significant noise sources do not exist within the TFO crossarray. The lack of reliable gain corrections precludes meaningful interpretation of any observed variations in absolute spectral level in terms of time and space stationarity.

To evaluate the structure of the ambient noise, analog bandpass filters were applied to both noise samples to isolate the contents of certain frequency bands. Appendix B displays the filtered noise samples.

---

*Texas Instruments Incorporated, 1966: Array Research Semiannual Tech. Rpt. No. 5, Sec. VII, AF33(657)-12747, 1 Jul.

A visual analysis was performed on the filtered data by measuring wavelet moveout along each arm of the TFO crossarray to determine wave velocity and direction. Examples of the stepout observed for the 0.0 cps to 0.20 cps energy is shown by the dots on Figure 18. By measuring the stepout along each leg of the TFO crossarray, it is possible to determine the apparent horizontal velocity and direction of the propagating mode.

The quiet noise sample exhibited energy in the 4-sec to 6-sec microseismic band on all three components. This energy is traveling toward approximately N37°E, with a velocity of 3.5 km/sec (Figure 18) and is observed to have approximately the same stepout on all components. Thus, it can be attributed to Rayleigh and Love wave energy propagating across the array. Frequency filtering of the windy noise sample (recorded several days earlier) displayed little evidence of low-velocity trapped-mode energy (Appendix B).

To investigate noise types and isotropy, coherence functions were computed at three locations using the resampled quiet noise (NSH-36). The locations selected were the Heber van and the TFO installations Z74 and Z63 — all of which lie on a N37°E line. A van was chosen for use in the coherence computation to investigate the feasibility of using van data for analysis. The Heber van was selected because it appeared to have more valid seismic data than did the other vans. At Heber and Z74, coherences were computed between vertical and radial, vertical and transverse, and radial and transverse components. Figures 19 and 20 display these coherences. Coherences also were computed between Heber and Z74 and between Z74 and Z63 for the respective vertical, radial and transverse components (Figures 21 and 22).

The ambient noise, although displaying very similar spectra at the TFO locations, was found to possess no significant coherence for a receiver separation of 10 km or greater (Figures 21 and 22), except for some highly coherent lines in the 4-sec to 6-sec range of the spectra for the quiet noise. Over the frequency range of interest, receiver separation was such that coherences significantly greater than zero could be expected only for a highly directional noise field or on horizontal instruments oriented along their separation vector (Figure 23).

The horizontal seismometer in line with the direction of propagation of the 4-sec to 6-sec energy shows a high coherence with the vertical seismometer in that frequency range, but the seismometer transverse to the energy has very small coherences with either (Figures 19 and 20). This is additional evidence that the energy is Rayleigh motion. The presence of Love wave energy on the transverse seismometer can be inferred from its lack of coherence with other seismometers.

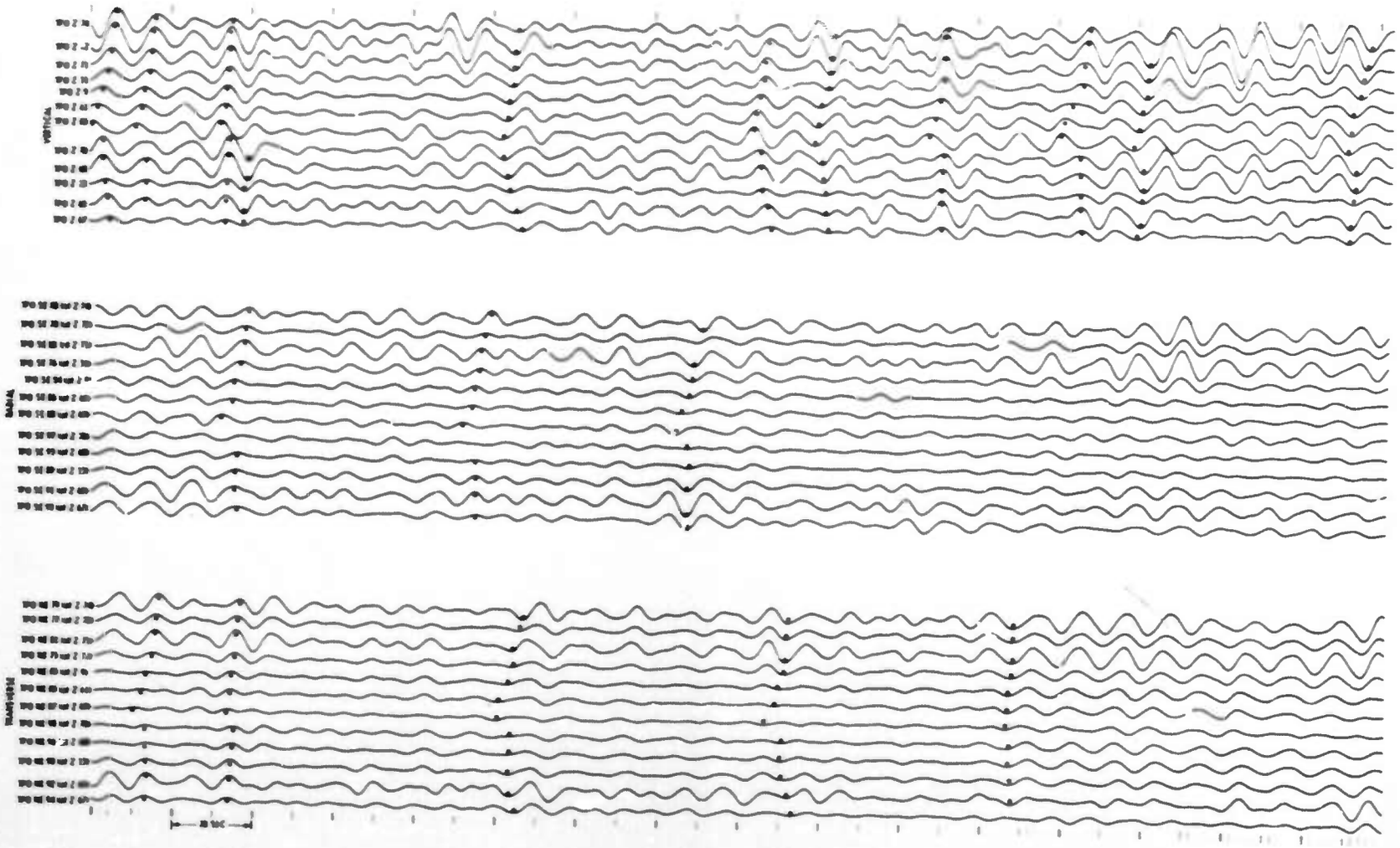

Figure 18. TFO Components of Quiet Noise Sample (NSH-36) with Bandpass Filter of 0.0 to 0.20 cps Applied

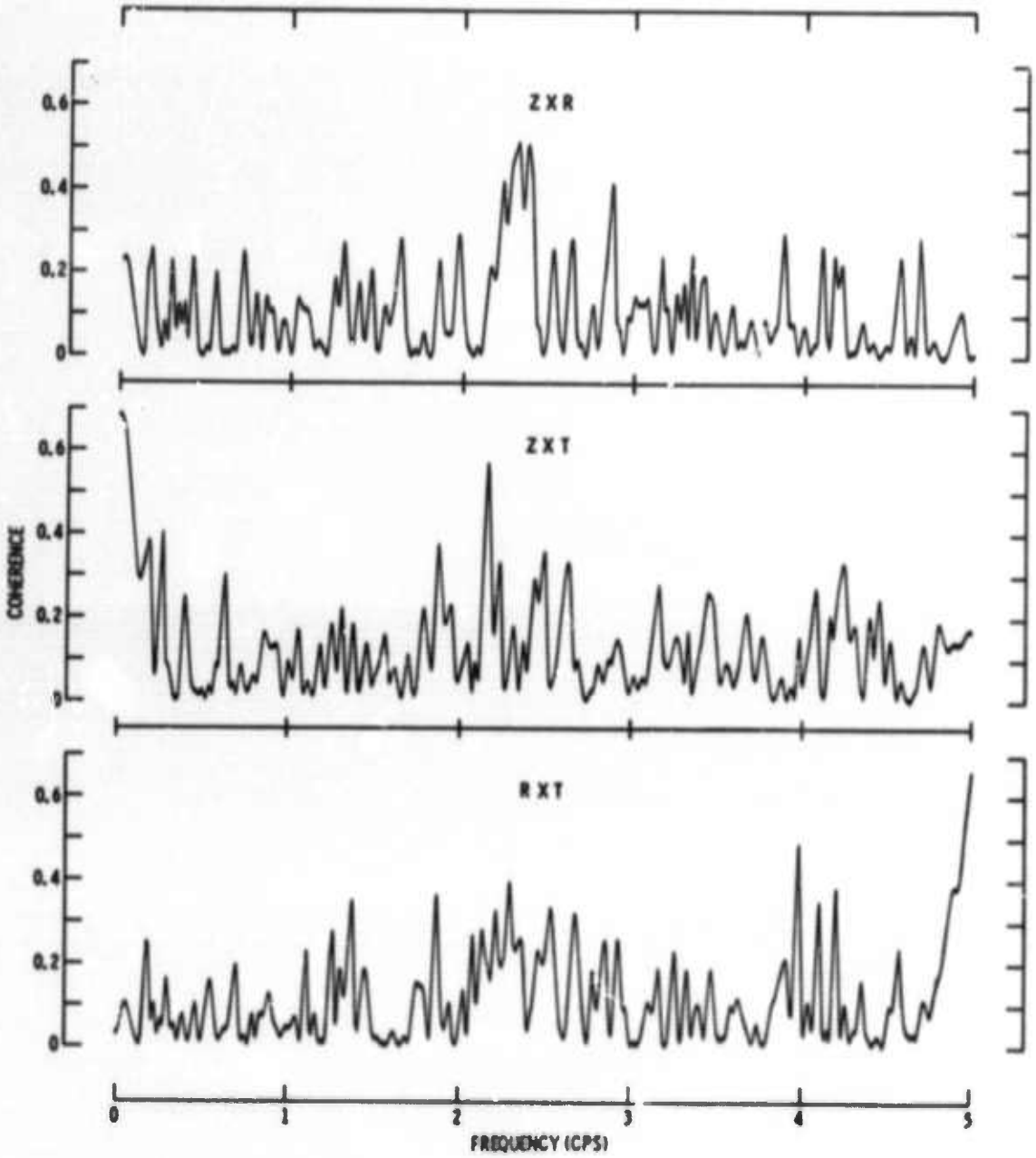

Figure 19. Coherences for Heber Van Between Vertical and Radial, Vertical and Transverse, and Radial and Transverse Components

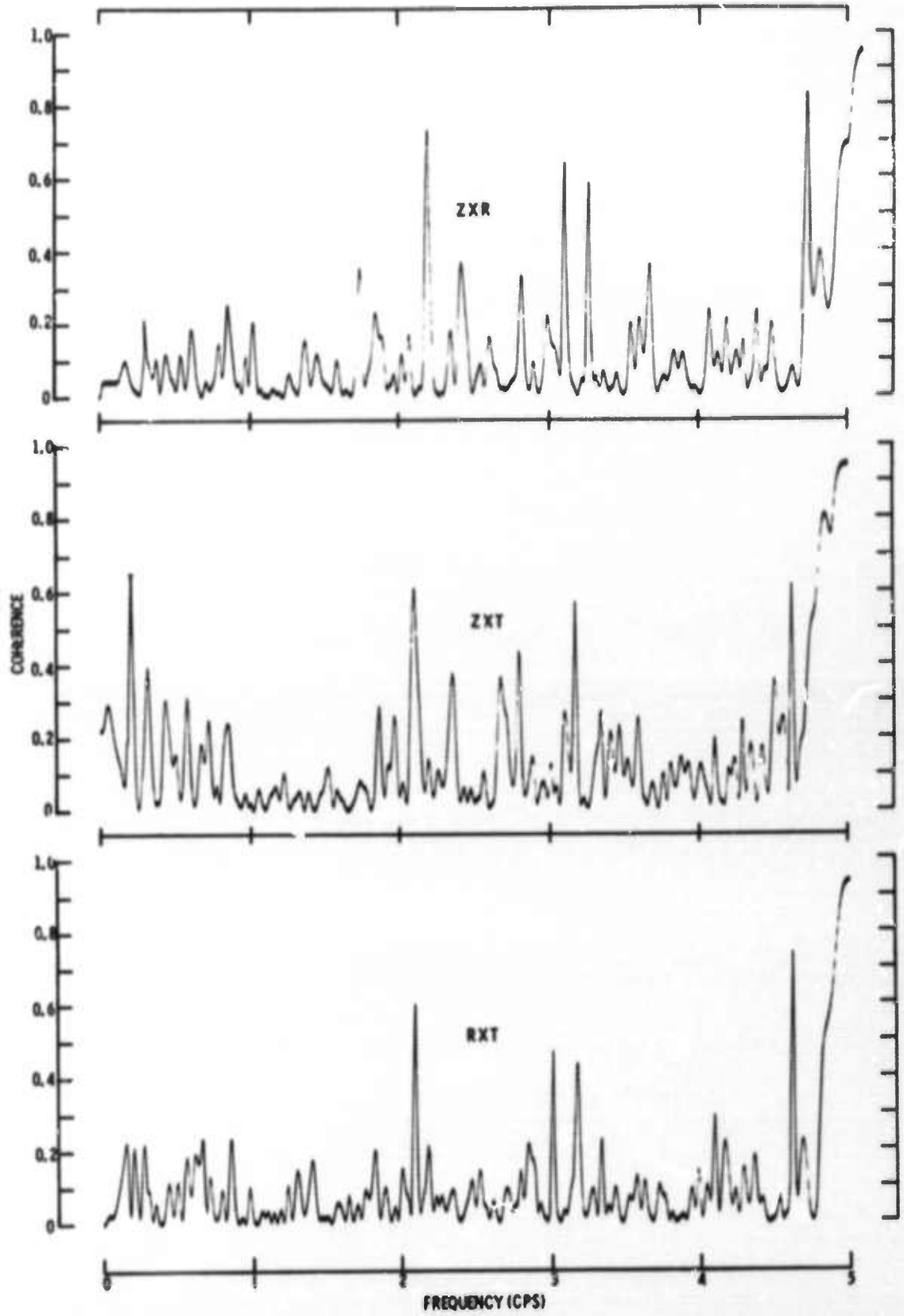

Figure 20. Coherences for Z74 Between Vertical and Radial, Vertical and Transverse and Radial and Transverse Components

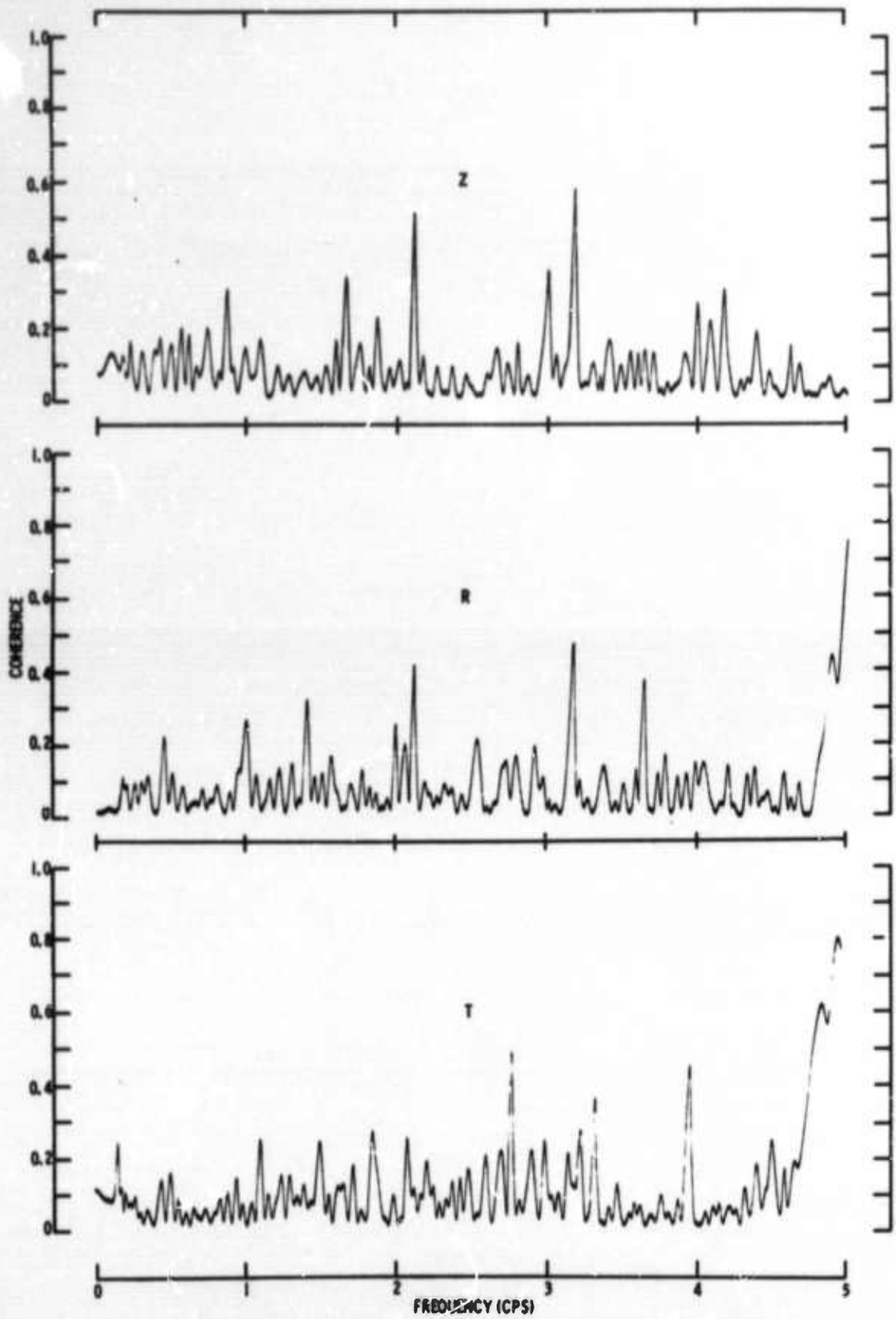

Figure 21. Coherences Between Heber Van and Z74 for Respective Vertical, Radial and Transverse Components

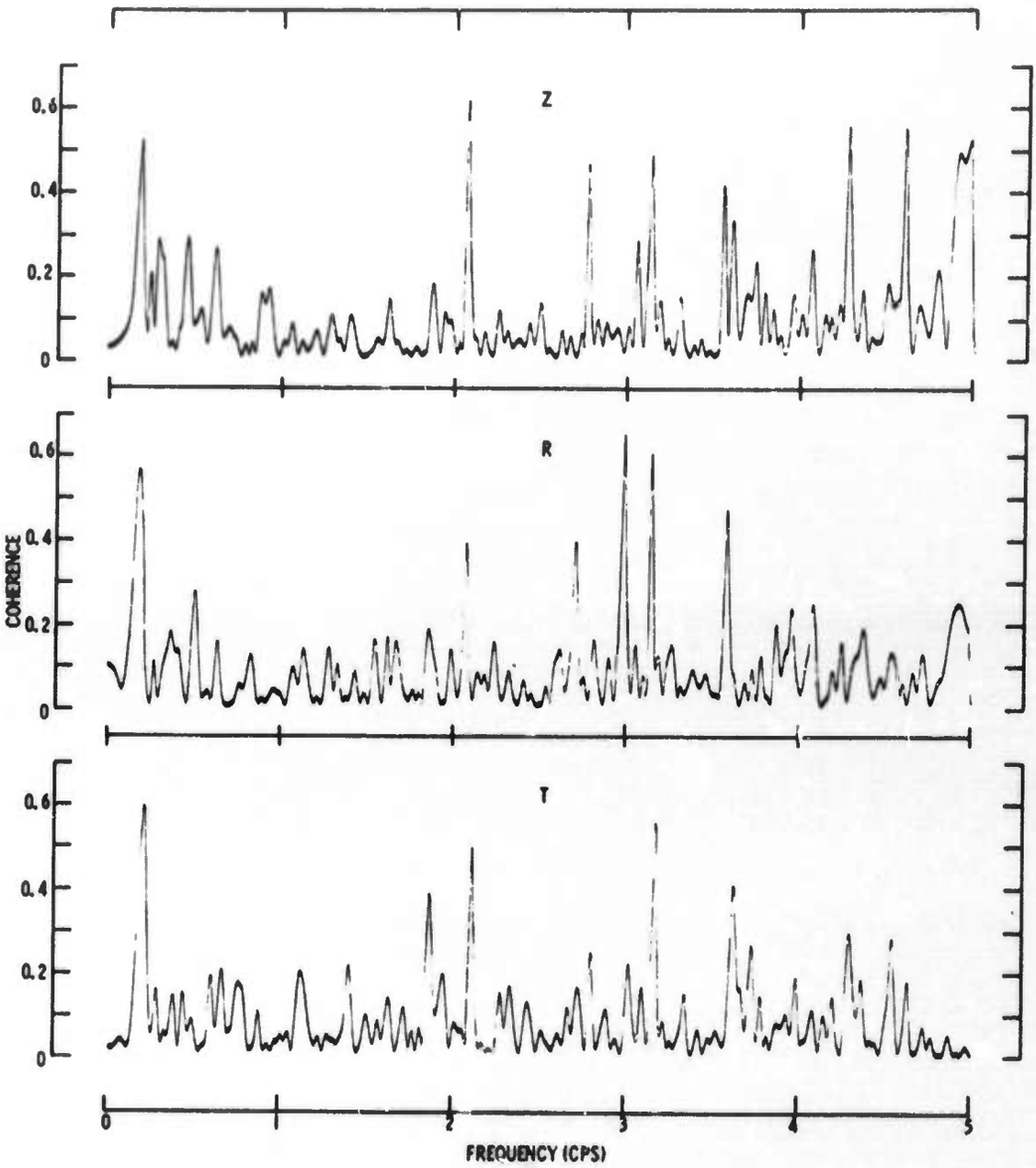

Figure 22. Coherences Between Z74 and Z63 for Respective Vertical, Radial and Transverse Components

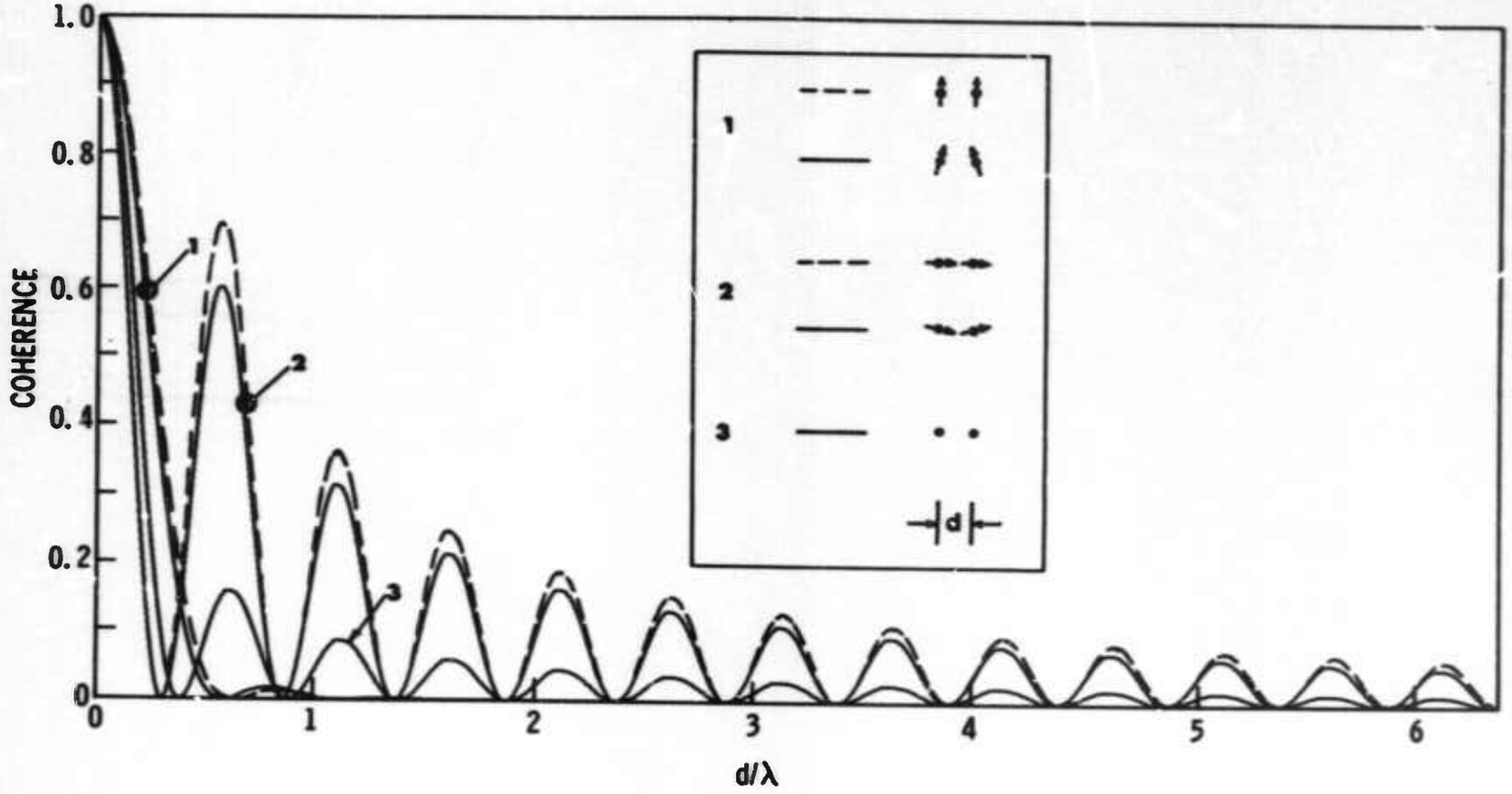

Figure 23. Theoretical 2-Channel Coherences for Isotropic Noise

It should be noted that, even in this highly directional noise field, the Heber van displayed less coherence than did the TFO, reflecting the impaired quality of the van data.

The Rayleigh and Love wave energy observed during the quiet noise sample was generated by tropical storm Emily, which was positioned off the lower coast of Baja California (Figure 24) during the recording of the noise sample. The higher-velocity energy is apparently bodywave energy and is present in both noise samples. The wind noise on the windy noise sample did not obscure the ambient noise and appears to be concentrated at approximately 0.4 cps in the spectrum. The bodywave energy is nonisotropic, coming from a predominantly southwest direction and traveling at velocities of 6 km/sec or greater in the frequency band of 0.25 to 1.2 cps.

This body wave energy can be grouped into two velocity ranges: 8 km/sec to 10 km/sec; and 14 km/sec or greater. Some of the 8 km/sec to 10 km/sec energy is possibly due to conversion of ocean waves to P and S phases on the western coast of Central and North America. The 14 km/sec or greater energy is probably due to the circum-Pacific belt of seismic activity.

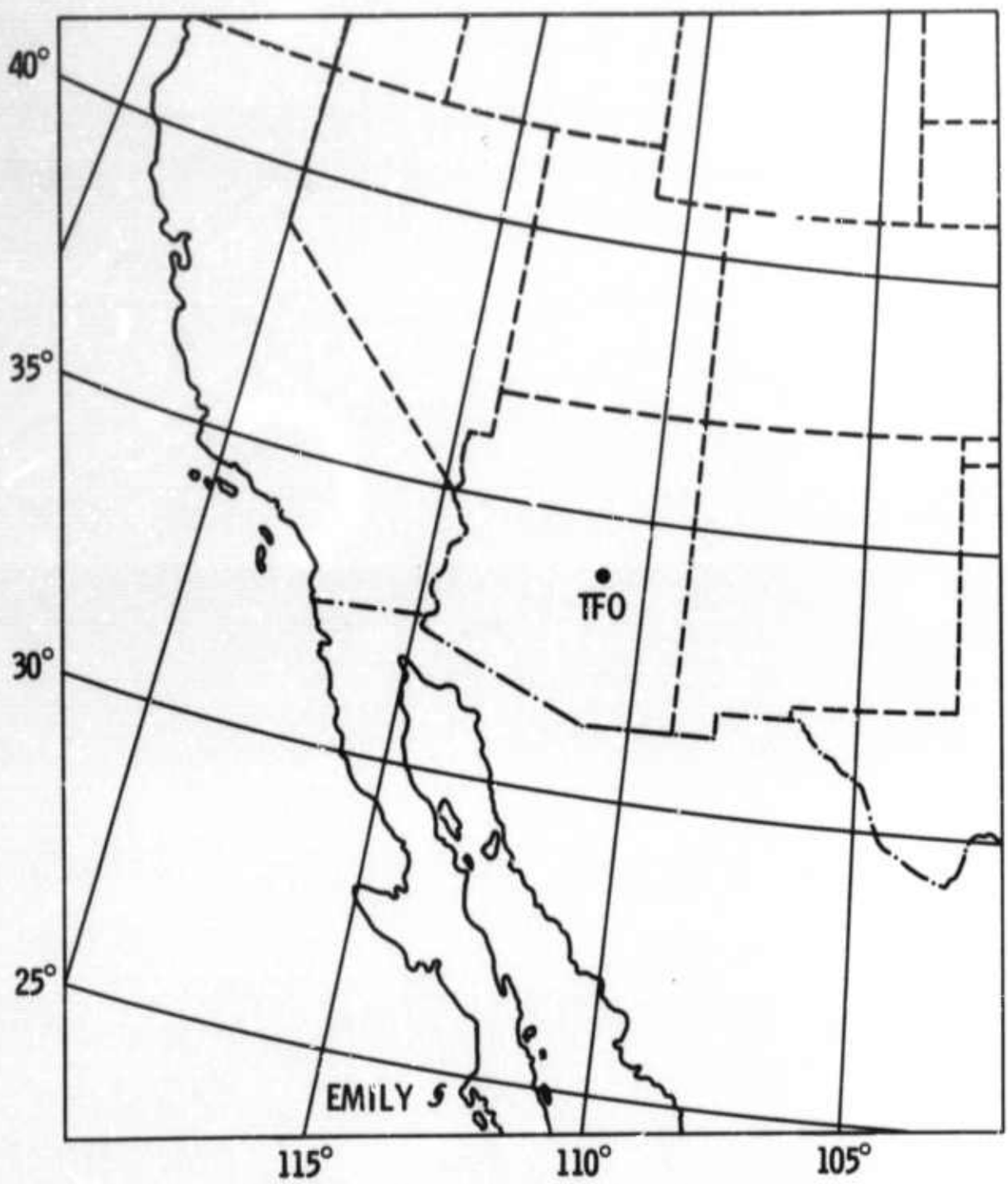

Figure 24. Location of Tropical Storm Emily at 1:00 a.m. EST 1 September 1965

SECTION VIII

RECOMMENDATIONS

Combining eight additional vans with the TFO array created an array of approximately 200-km aperture, making it possible for large variations to exist in the ambient noise field (particularly trapped-mode components) over the array. However, the discovery that the van data are of little seismic validity effectively reduces the array to a 10-km aperture centered at TFO. Thus, the probability of significant variations in the noise field is considerably reduced.

The lack of reliable gain corrections precludes interpretation of any variations in the noise field on an absolute spectral basis, but the noise field at the TFO array already has been investigated several times on a spectral basis.*

Therefore, further spectral analysis with these data does not appear to be justified. A possible exception might involve the use of some or all of the van data at the lower end of the frequency band where system noise appears to be less of a problem. However, attempts to use the van data for this report have met with little success and further use is recommended only with careful interpretation and a full realization of the limitations of the data.

The coherence of the field at TFO has been investigated previously** for vertical components and for a single 3-component group. Since coherence functions are independent of gain variations, the present data may be used for further investigation of the noise field coherence on a 3-component basis for receiver separations from 1 to 10 km.

---

*Wherry, M.S., 1965: Noise Analysis for Tonto Forest Seismological Observatory, Tech. Rpt. - TFSO, Texas Instruments Incorporated, 16 Aug.

Texas Instruments Incorporated, 1965: Array Research Semiannual Tech. Rpt. No. 2, AF 33(657)-12747, 15 Nov.

Texas Instruments Incorporated, 1965: Array Research Semiannual Tech. Rpt. No. 3, AF 33(657)-12747, 3 Jun.

**Ibid, Semiannual Tech. Rpt. No. 3, Sec. V.

APPENDIX A
POWER DENSITY SPECTRA

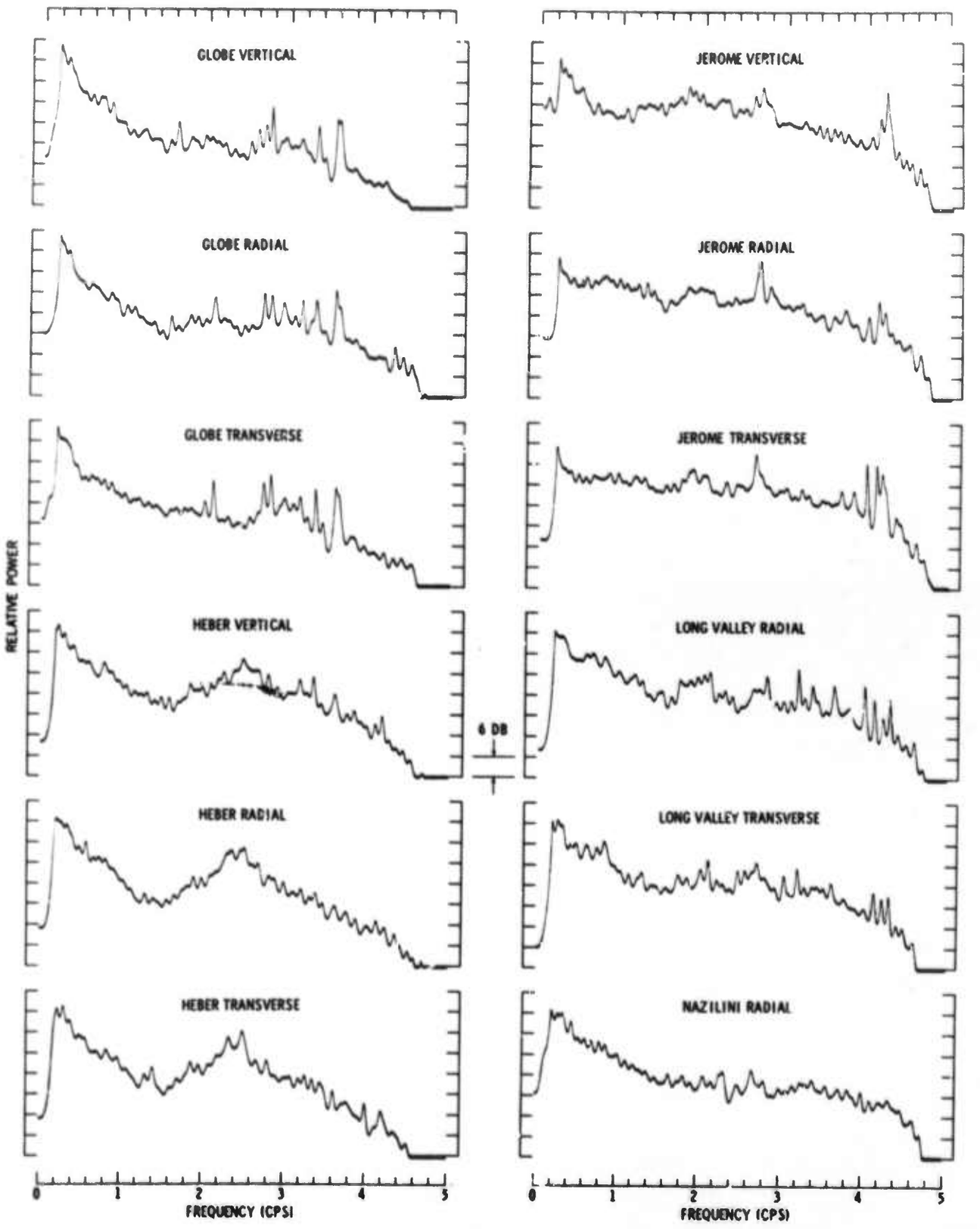

Figure A-1. Quiet Noise Power Density Spectra

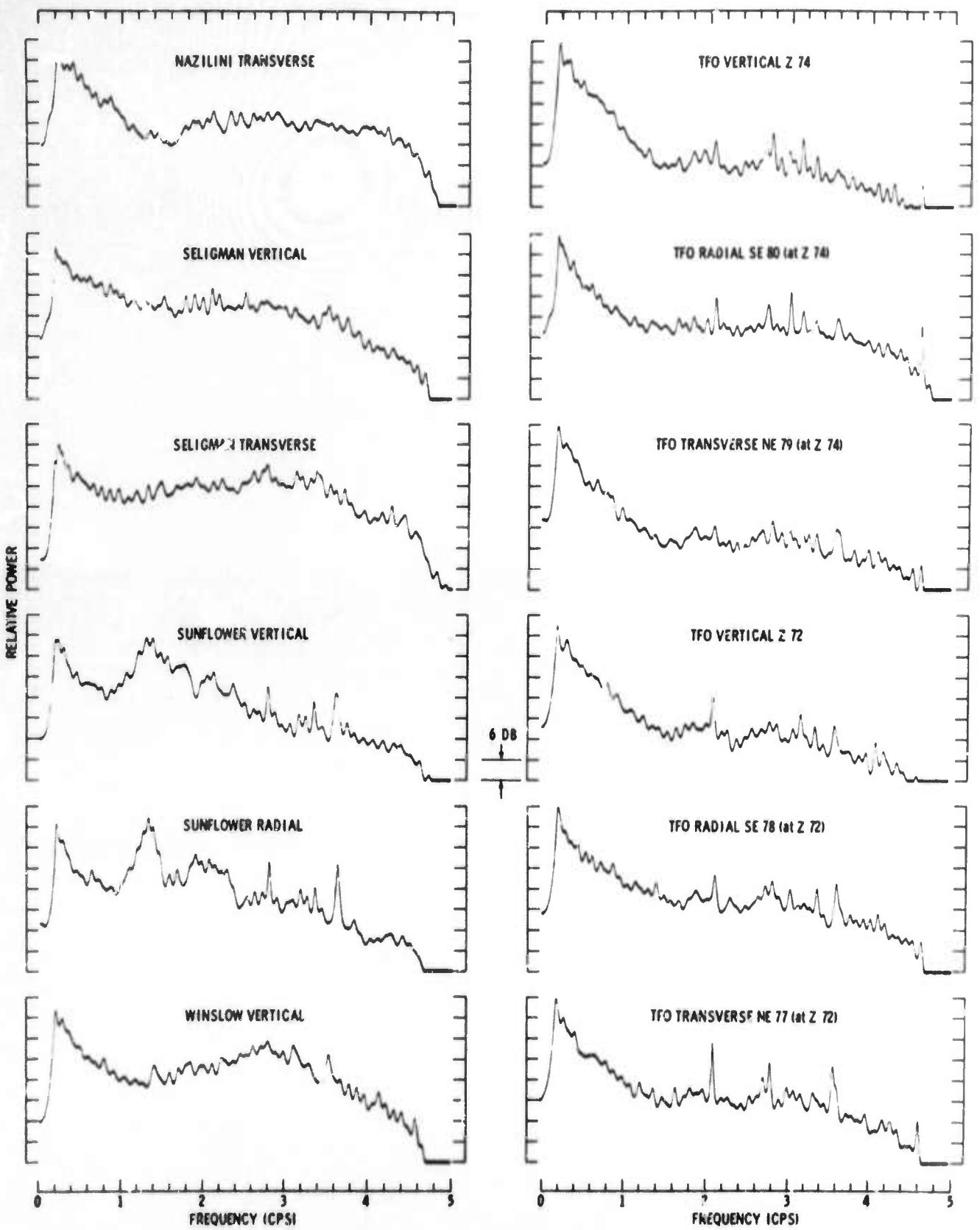

Figure A-2. Quiet Noise Power Density Spectra

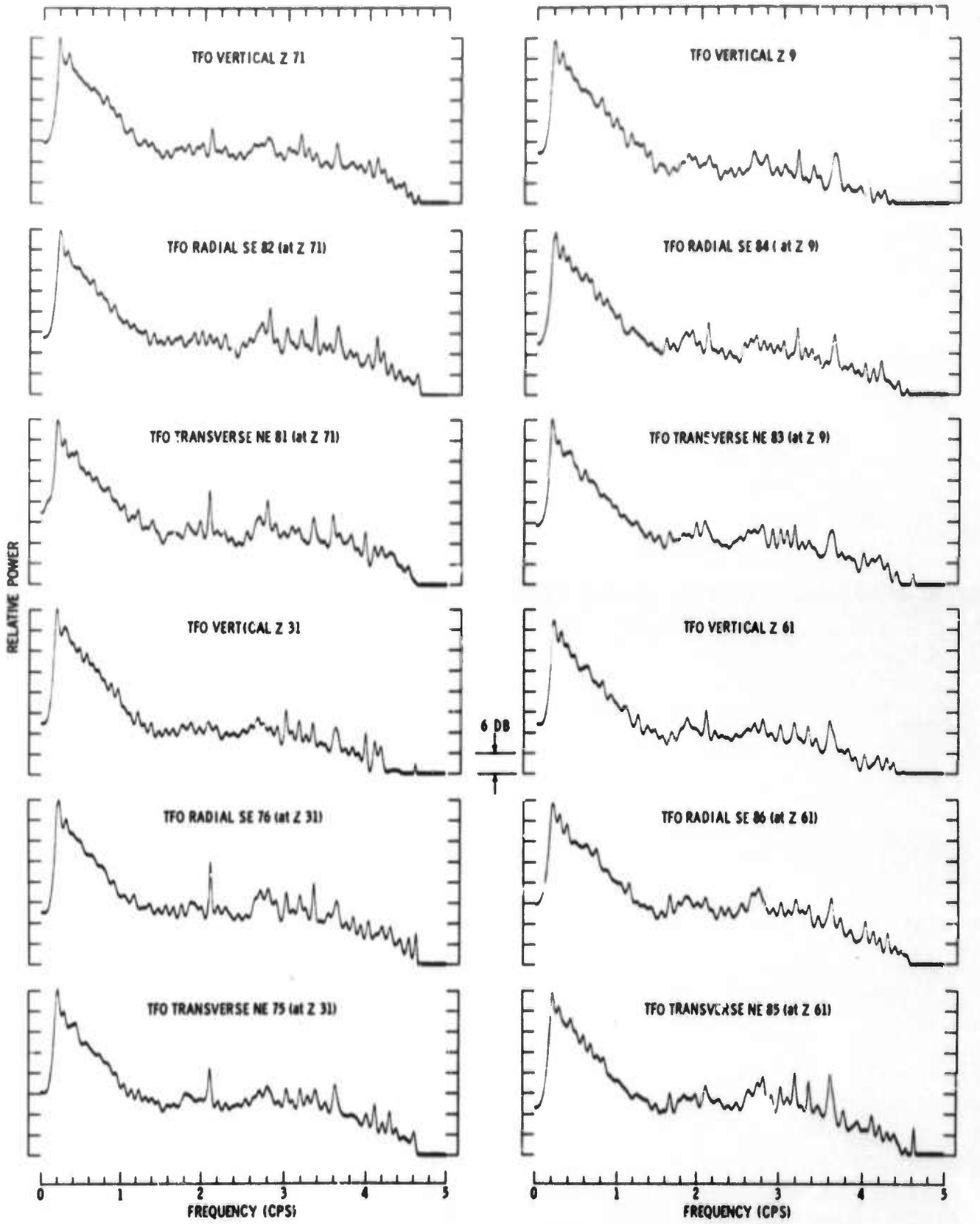

Figure A-3. Quiet Noise Power Density Spectra

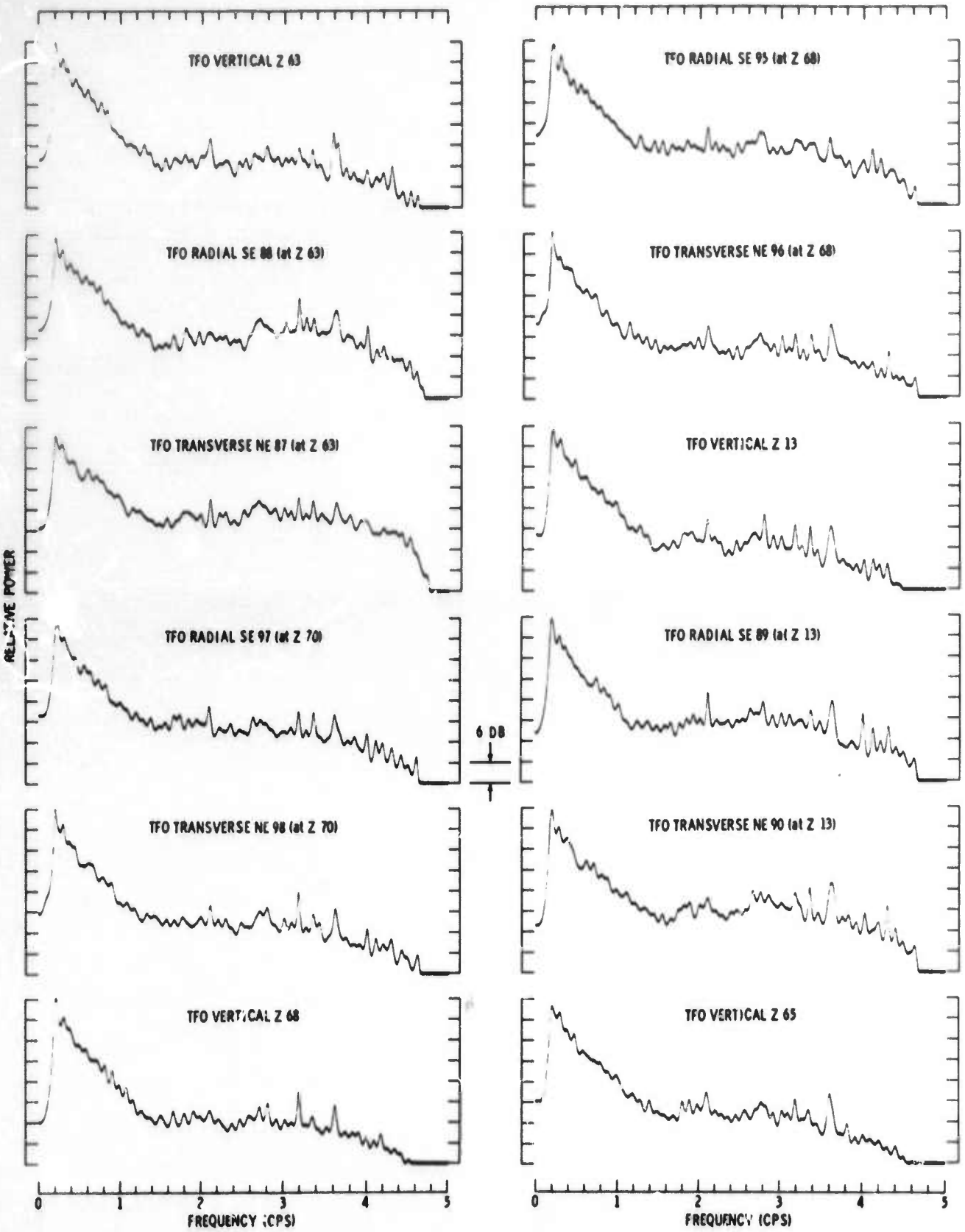

Figure A-4. Quiet Noise Power Density Spectra

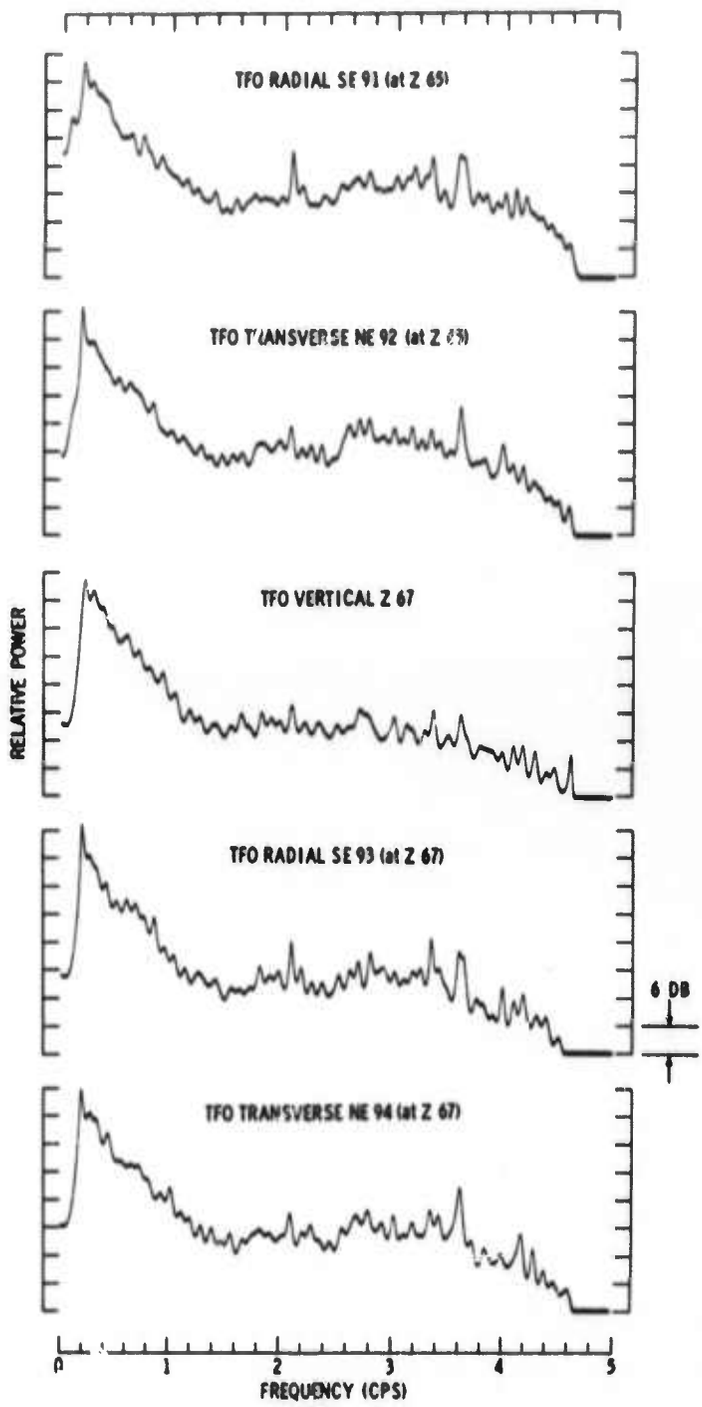

Figure A-5. Quiet Noise Power Density Spectra

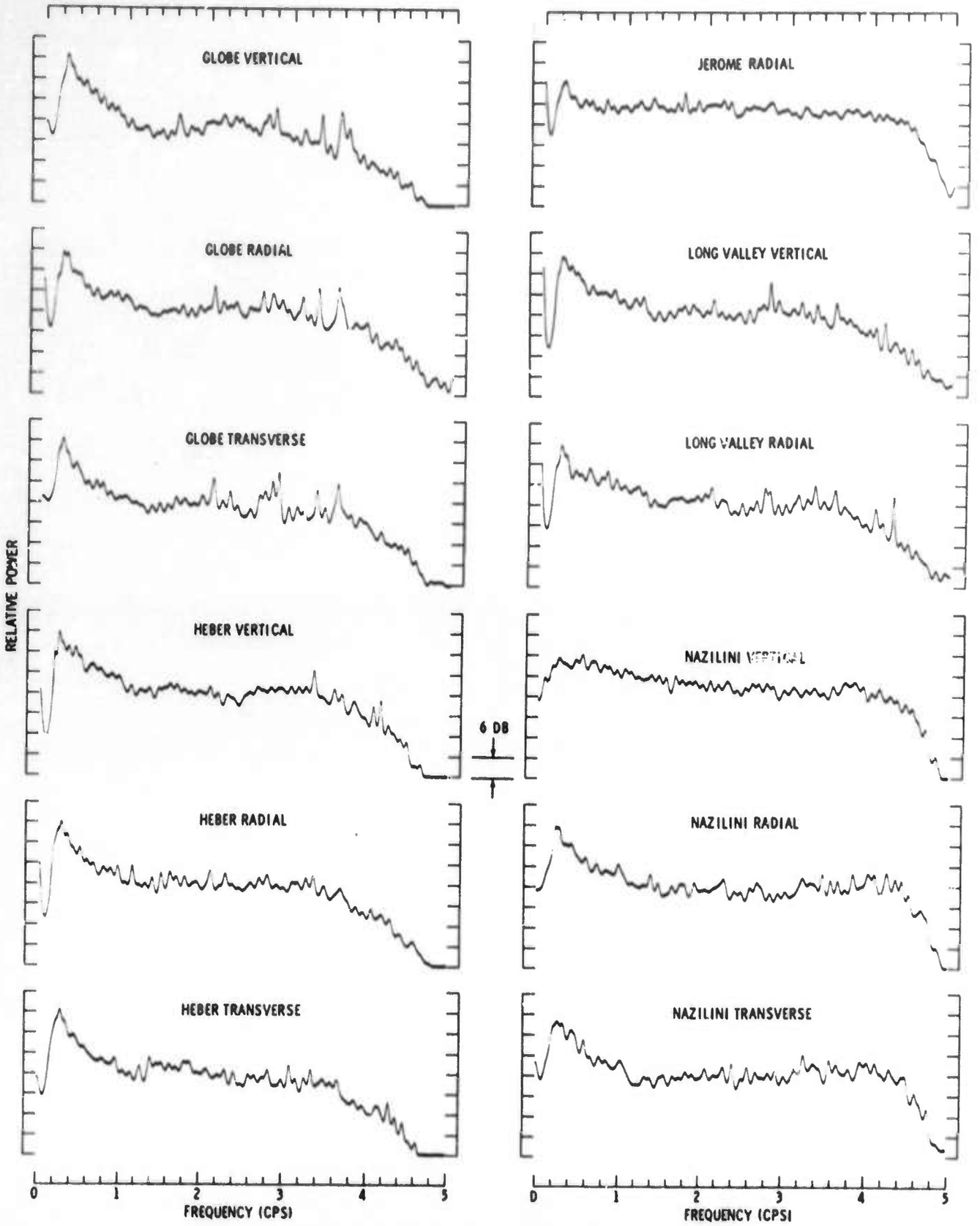

Figure A-6. Windy Noise Power Density Spectra

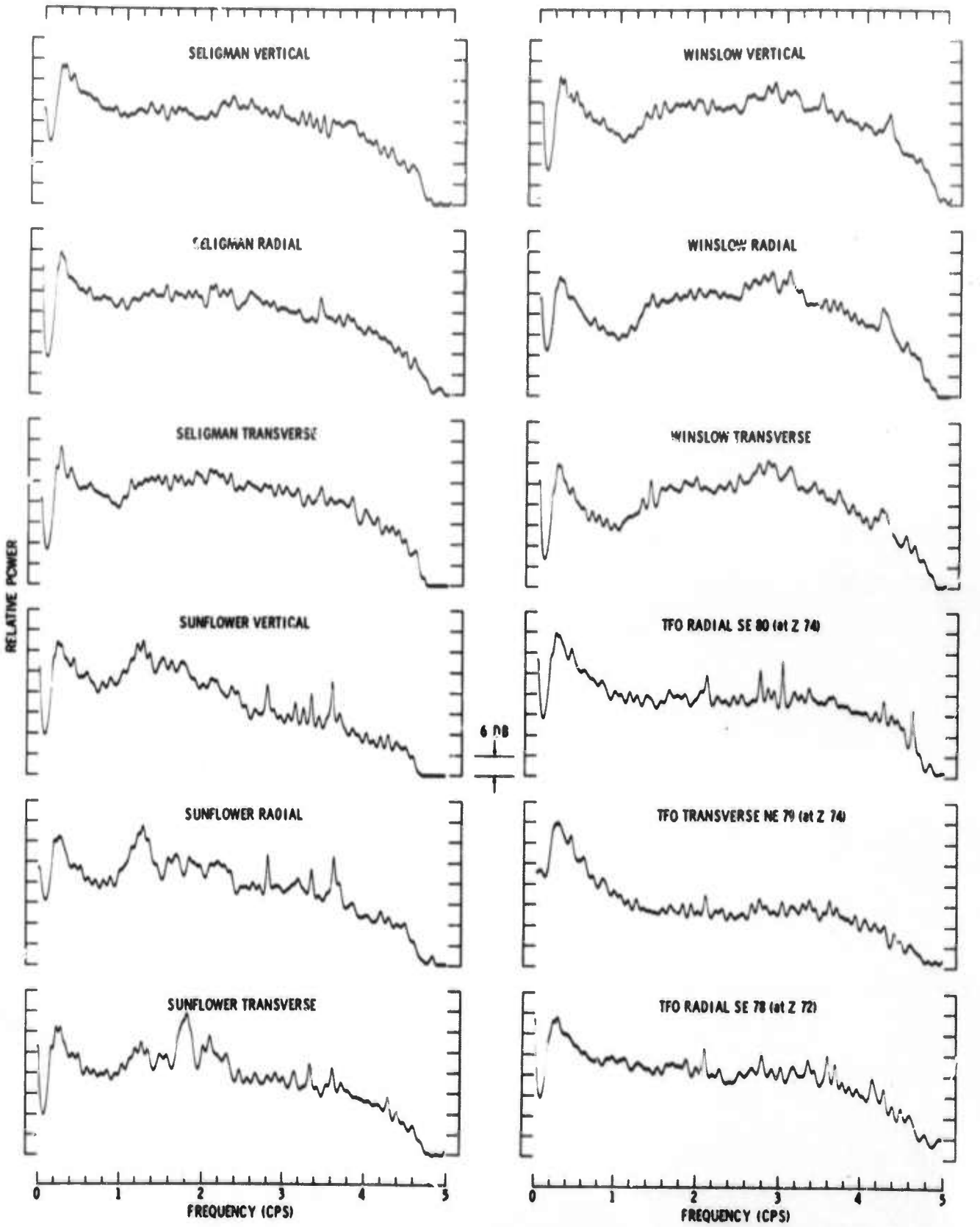

Figure A-7. Windy Noise Power Density Spectra

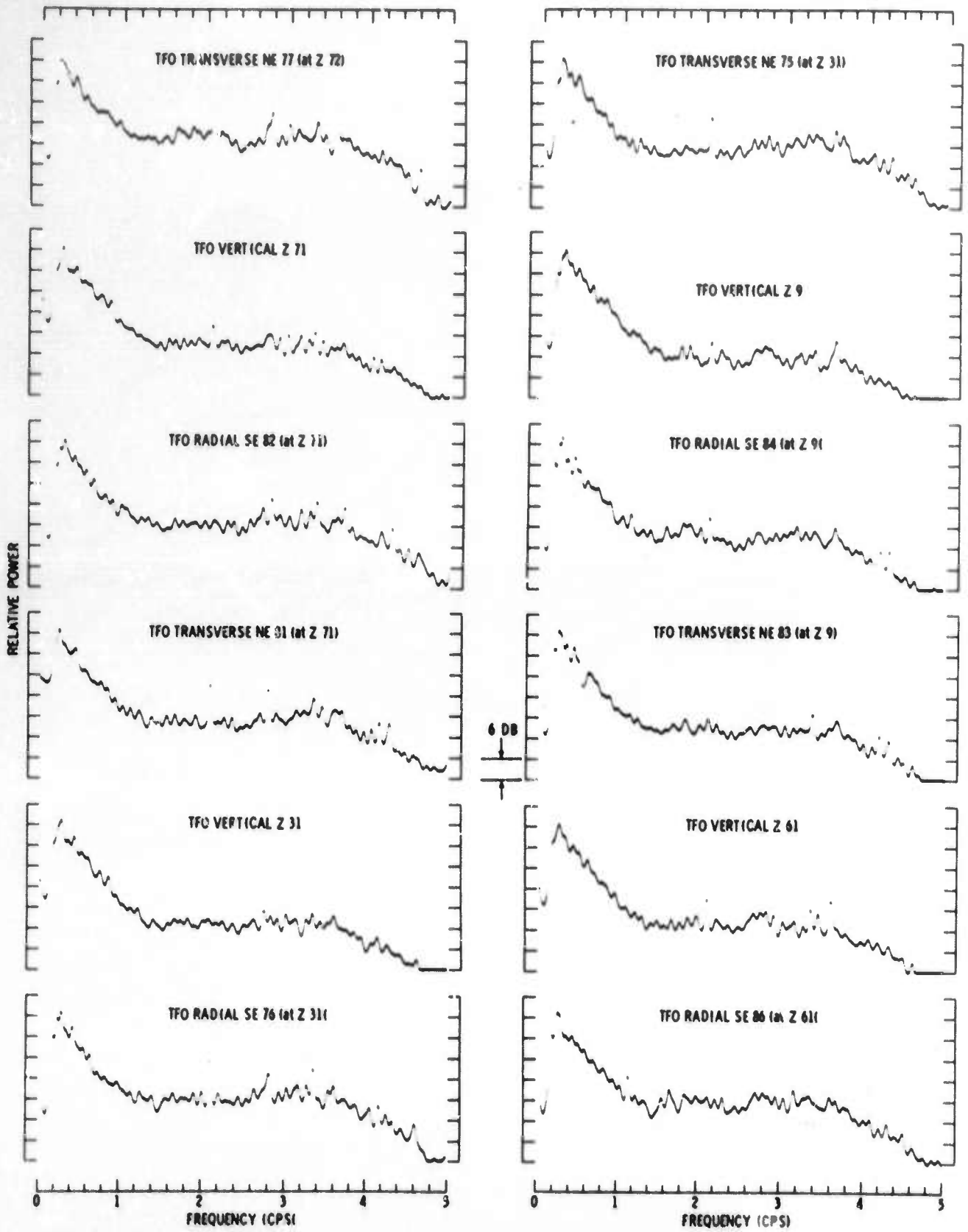

Figure A-8. Windy Noise Power Density Spectra

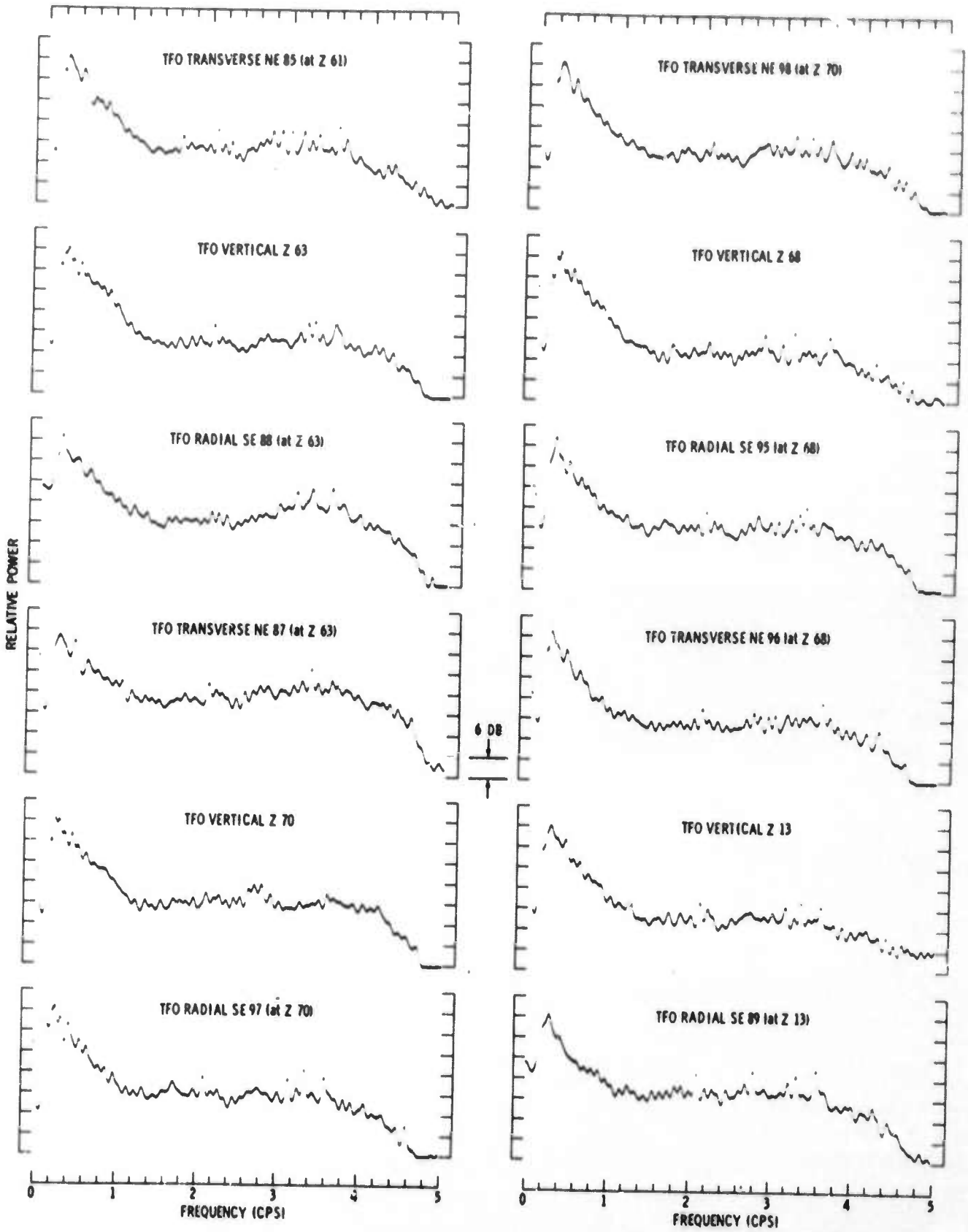

Figure A-9. Windy Noise Power Density Spectra

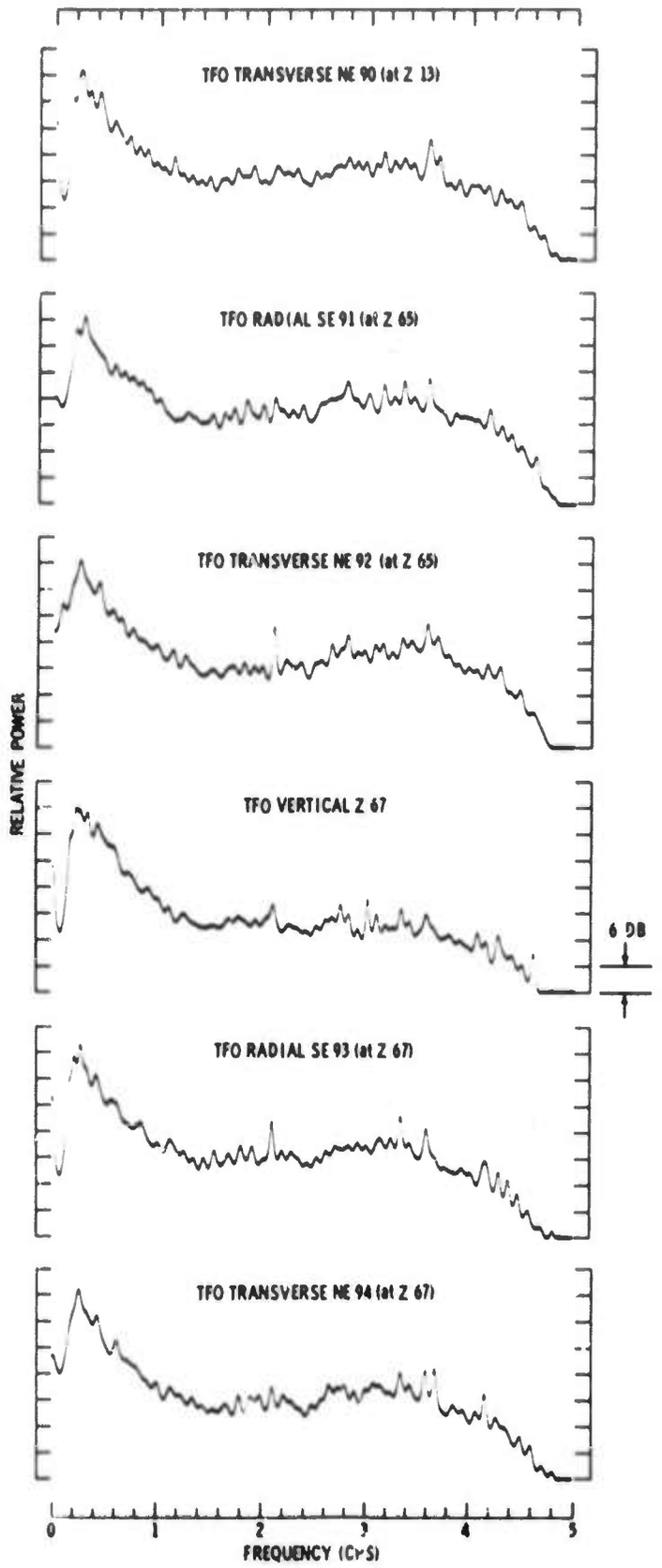

Figure A-10. Windy Noise Power Density Spectra

APPENDIX B
FREQUENCY FILTERING

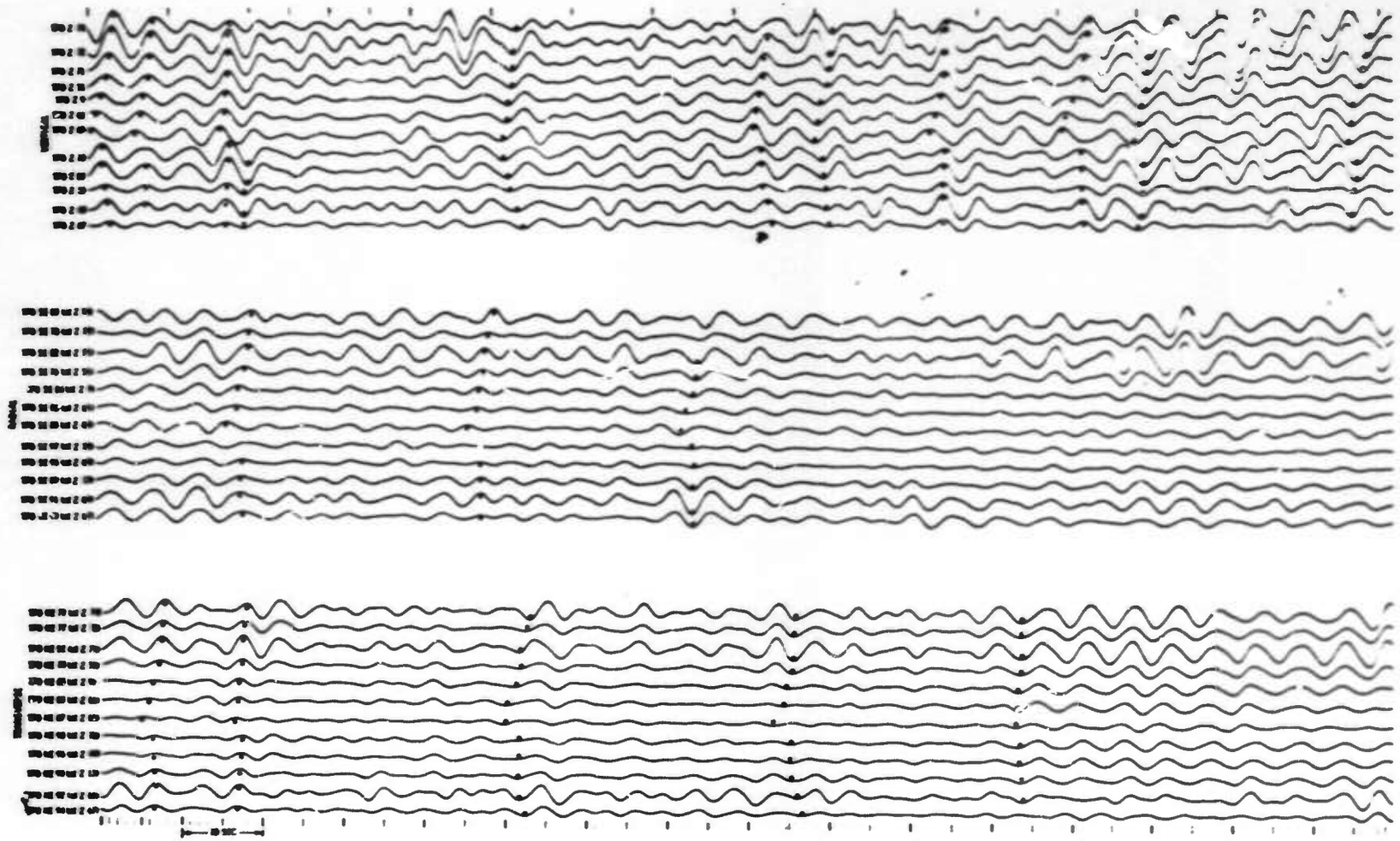

Figure B-1. TFO Components of Quiet Noise Sample (NSH-36) with Bandpass Filter of 0.0 to 0.20 cps Applied

Figure B-2. TFO Components of Quiet Noise Sample (NSH-36) with Bandpass Filter of 0.21 to 0.57 cps Applied

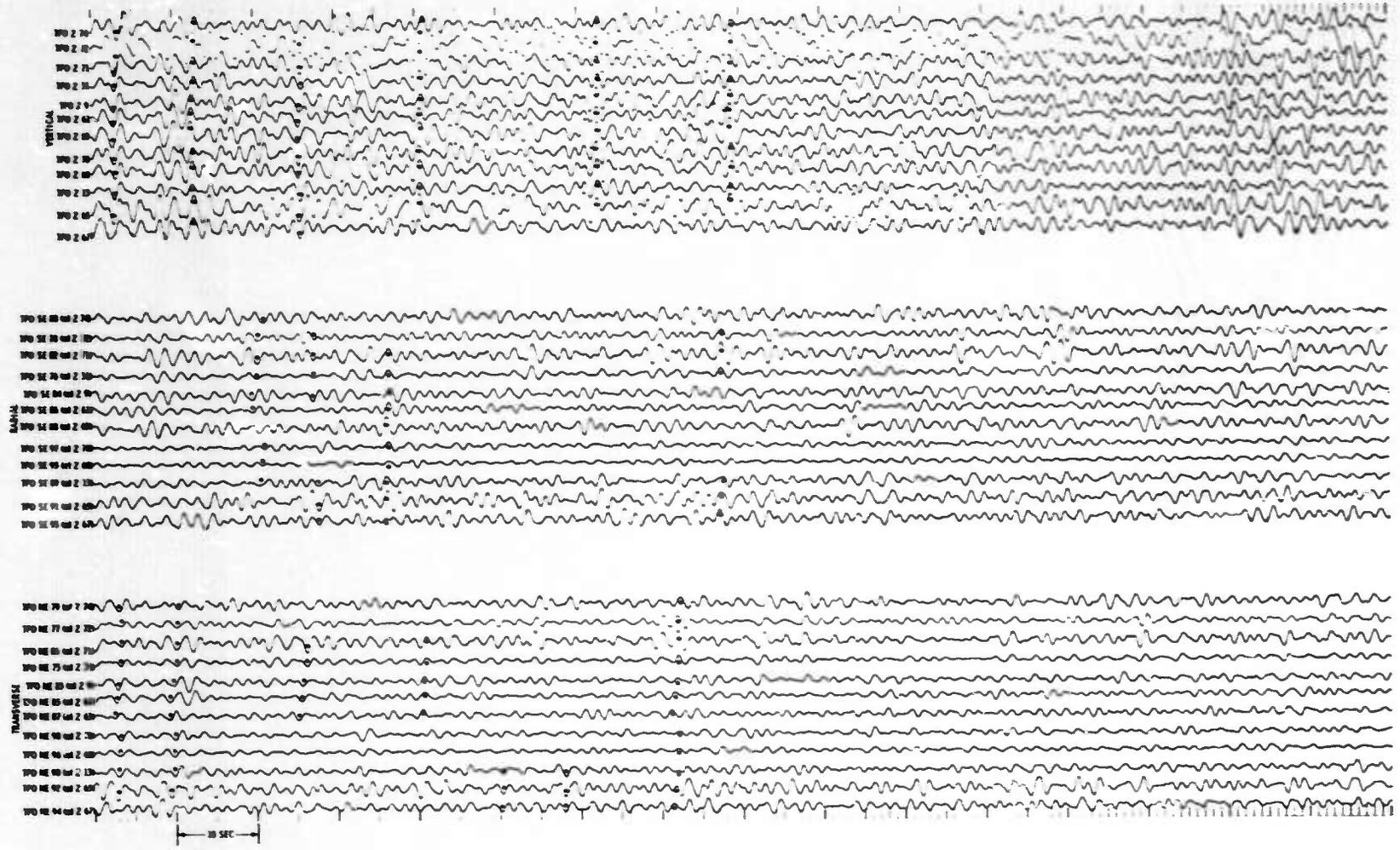

Figure B-3. TFO Components of Quiet Noise Sample (NSH-36) with Bandpass Filter of 0.48 to 0.92 cps Applied

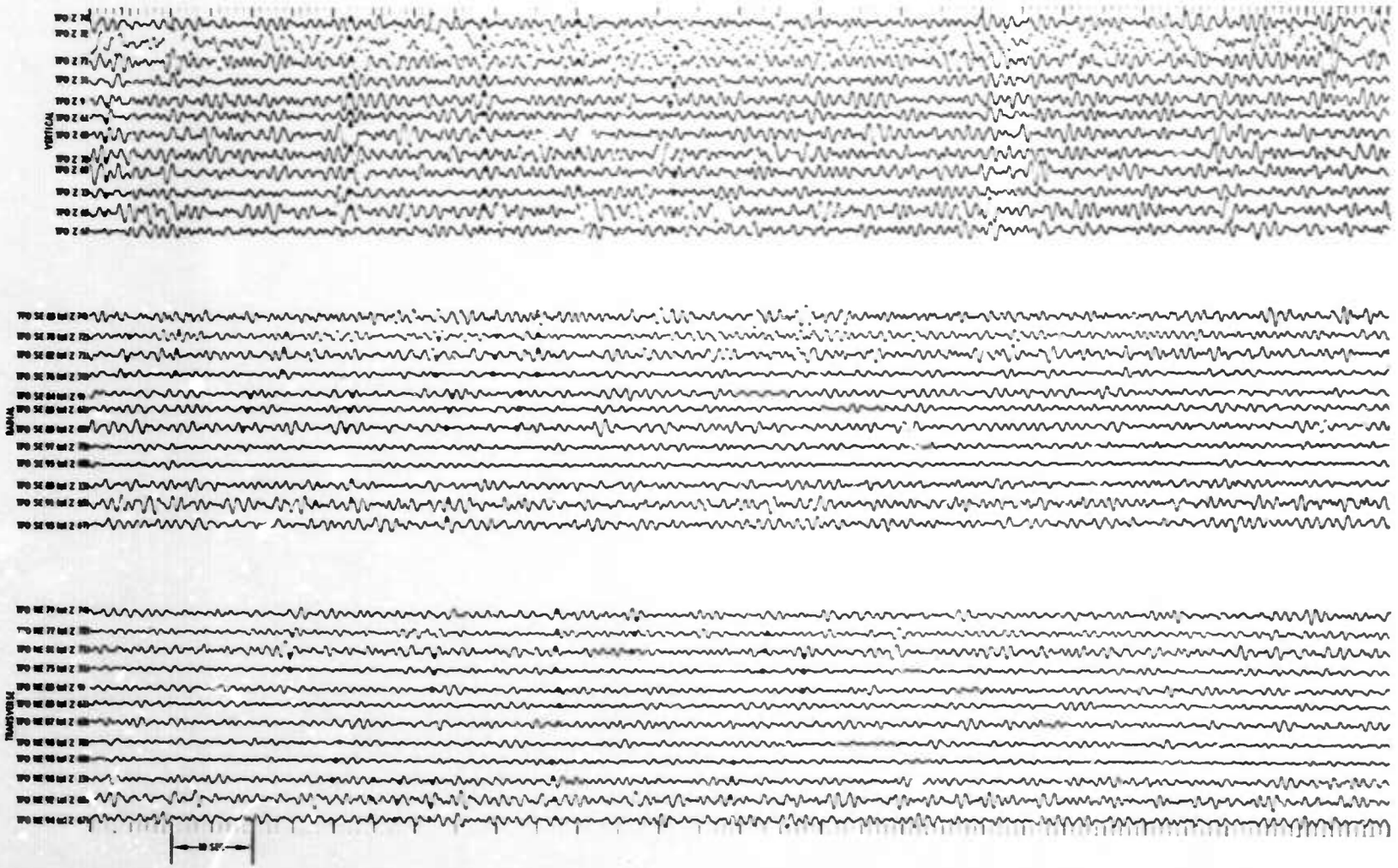

Figure B-4. TFO Components of Quiet Noise Sample (NSH-36) with Bandpass Filter of 0.90 to 1.20 cps Applied

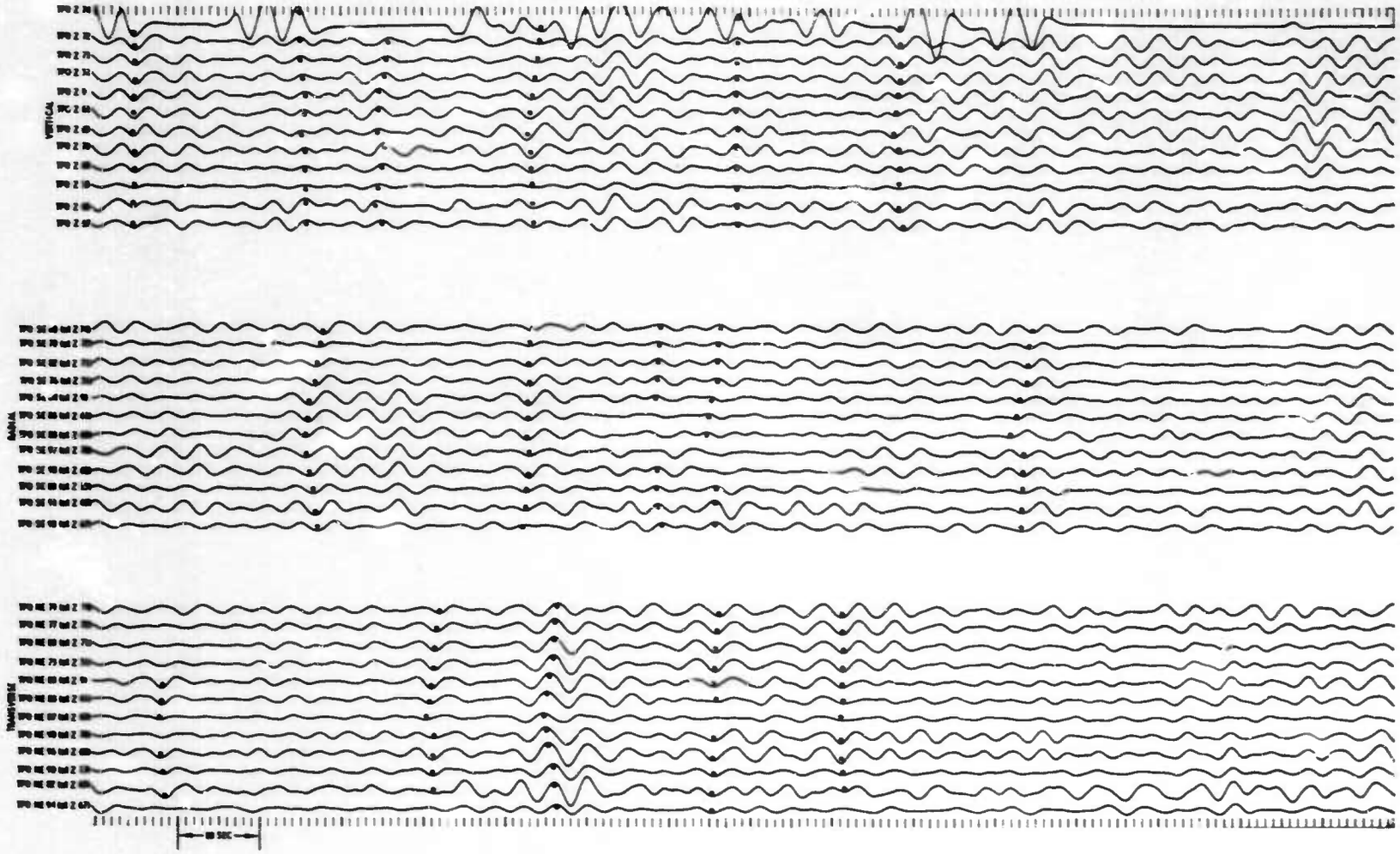

Figure B-5. TFO Components of Windy Noise Sample (NSH-1F) with Bandpass Filter of 0.0 to 0.20 cps Applied

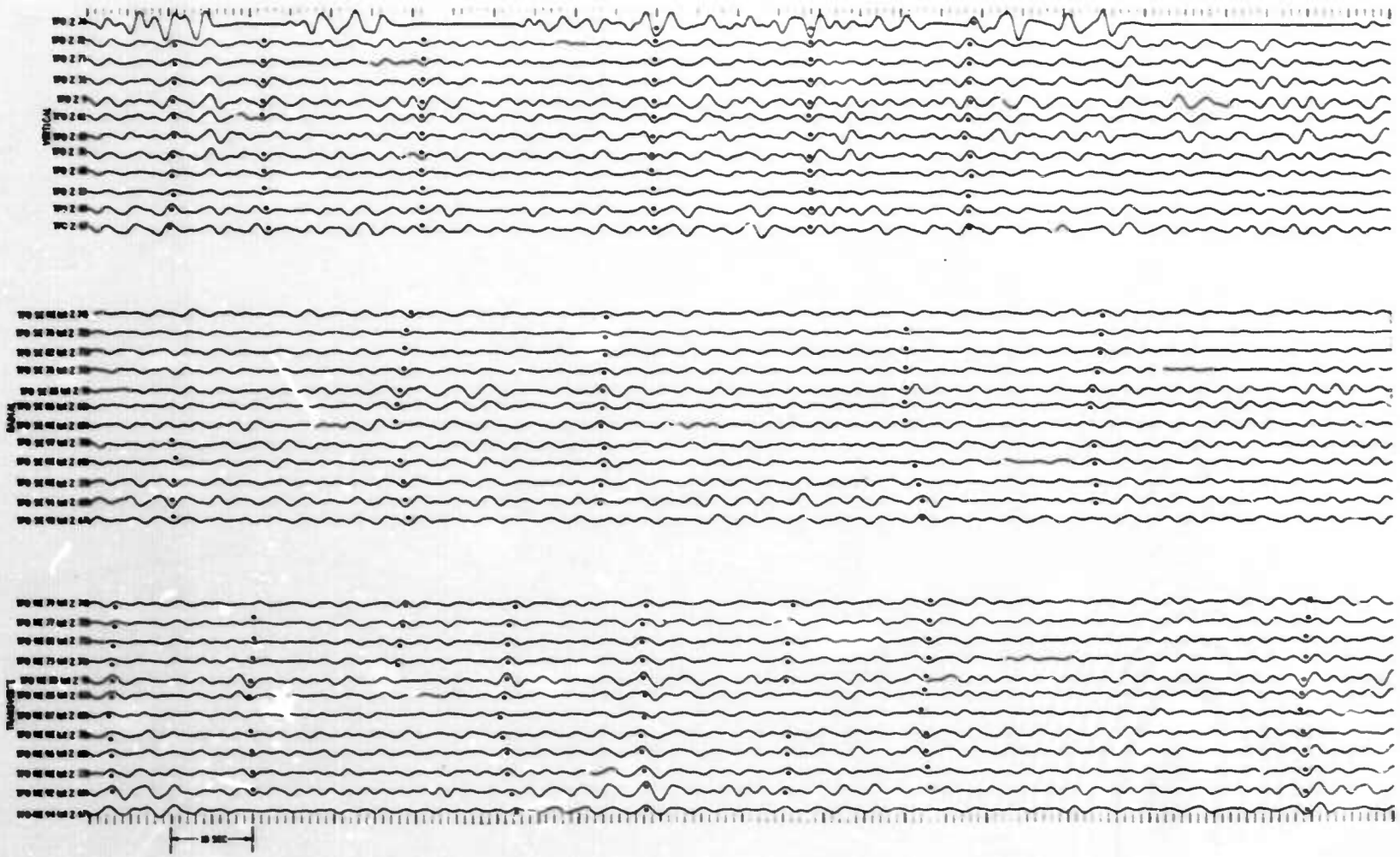

Figure B-6. TFO Components of Windy Noise Sample (NSH-1F) with Bandpass Filter of 0.21 to 0.57 cps Applied

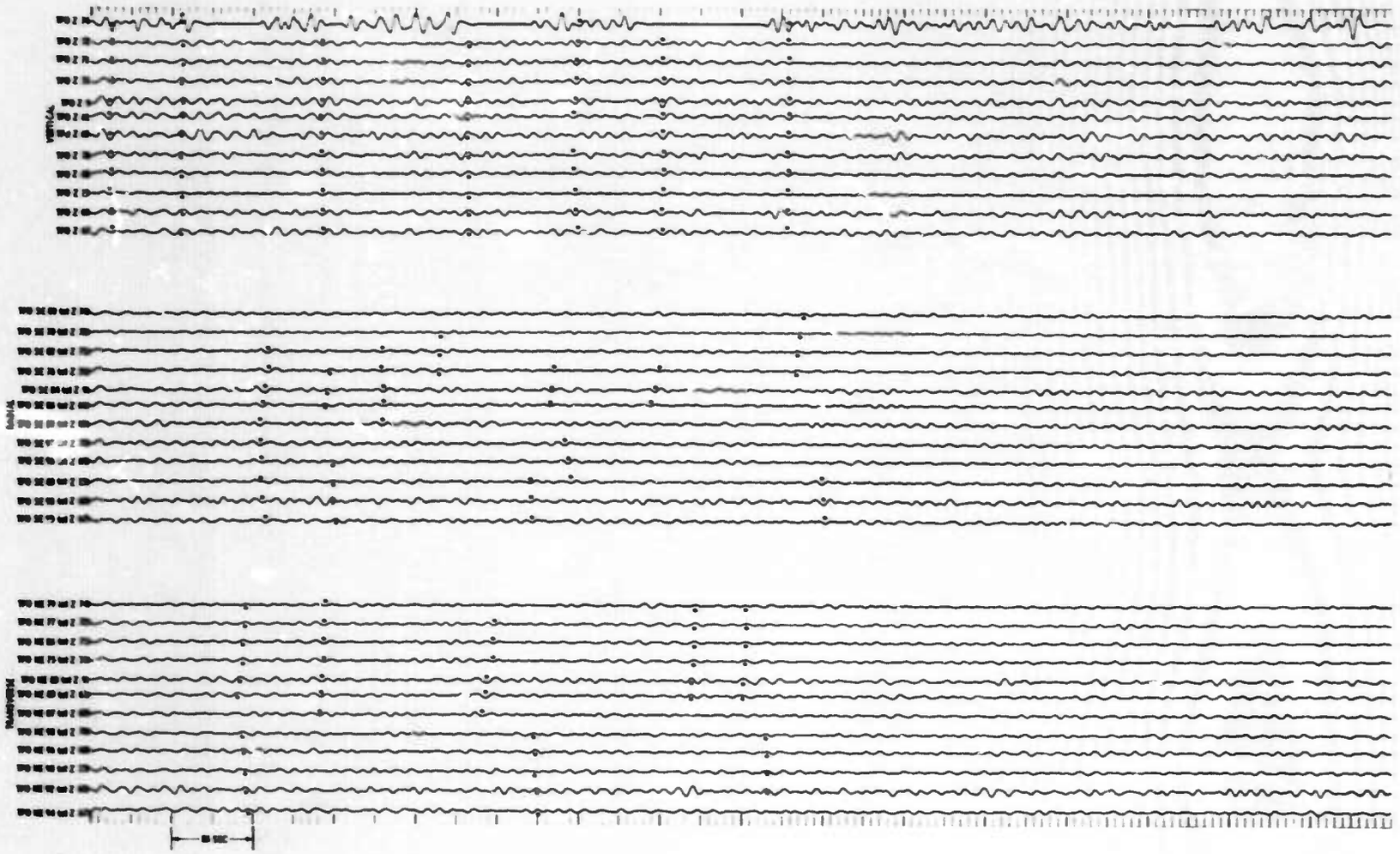

Figure B-7. TFC Components of Windy Noise Sample (NSH-1F) with Bandpass Filter of 0.48 to 0.92 cps Applied

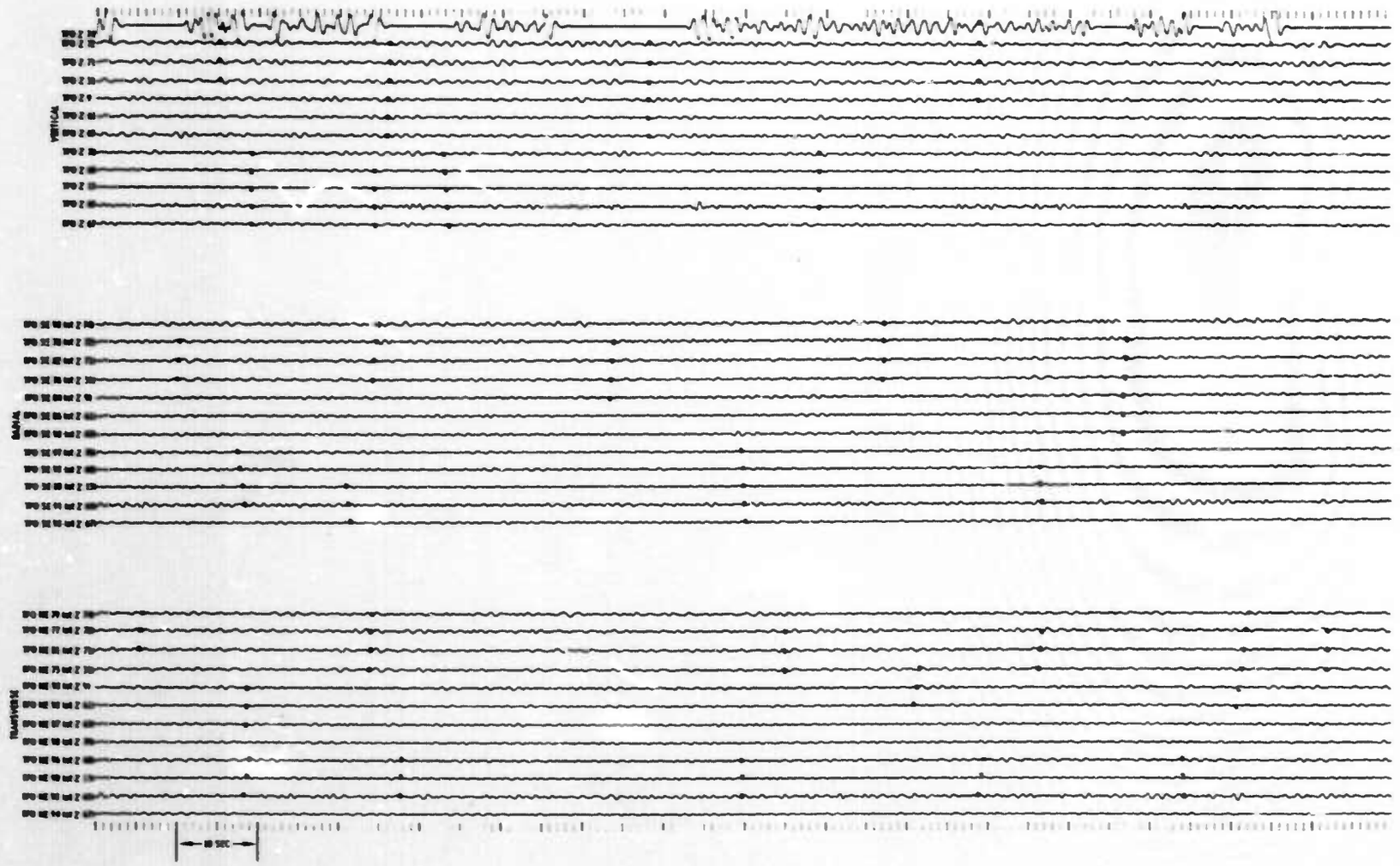

Figure B-8. TFO Components of Windy Noise Sample (NSH-1F) with Bandpass Filter of 0.90 to 1.20 cps Applied